

Direct simulation of interfacial waves in a high-viscosity-ratio and axisymmetric core–annular flow

By RUNYUAN BAI¹, KANCHAN KELKAR²
AND DANIEL D. JOSEPH¹

¹Department of Aerospace Engineering and Mechanics, University of Minnesota,
Minneapolis, MN 55455, USA

²Innovative Research, Inc., 2800 University Avenue SE, Minneapolis,
MN 55414, USA

(Received 3 May 1995 and in revised form 29 May 1996)

A direct numerical simulation of spatially periodic wavy core flows is carried out under the assumption that the densities of the two fluids are identical and that the viscosity of the oil core is so large that it moves as a rigid solid which may nevertheless be deformed by pressure forces in the water. The waves which develop are asymmetric with steep slopes in the high-pressure region at the front face of the wave crest and shallower slopes at the low-pressure region at the lee side of the crest. The simulation gives excellent agreement with the experiments of Bai, Chen & Joseph (1992) on up flow in vertical core flow where axisymmetric bamboo waves are observed. We define a threshold Reynolds number and explore its utility; the pressure force of the water on the core relative to a fixed reference pressure is negative for Reynolds numbers below the threshold and is positive above. The wave length increases with the hold-up ratio when the Reynolds number is smaller than a second threshold and decreases for larger Reynolds numbers. We verify that very high pressures are generated at stagnation points on the wavefront. It is suggested that a positive pressure force is required to levitate the core off the wall when the densities are not matched and to centre the core when they are. A further conjecture is that the principal features which govern wavy core flows cannot be obtained from any theory in which inertia is neglected.

1. Introduction

Lubricated pipelining of viscous materials such as heavy crude, slurries and capsules is robustly stable and has a high economic potential. The viscous material does not touch the wall. In the case of crude oil, the drag reduction which can be achieved by lubrication is of the order of the viscosity ratio with increased throughputs of ten thousand or more (for more background see Joseph & Renardy 1993). These lubricated flows are called core flows because the viscous material flows in a core lubricated all around by water.

Probably the most important industrial pipeline to date was the 6-inch (15.2 cm) diameter, 24-mile (38.6 km) long Shell line from the North Midway Sunset Reservoir near Bakersfield, California, to the central facilities at Ten Section. The line was run under the supervision of Veet Kruka for 12 years from 1970 until the Ten section was closed. When lubricated by water at a volume flow rate of 30% of the total, the pressure drop varied between 900 p.s.i. and 1100 p.s.i. at a flow rate of 24000 barrels

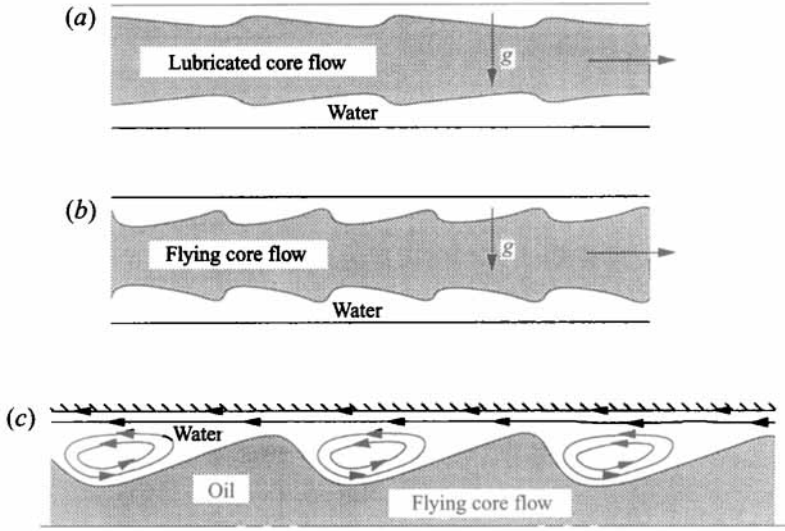


FIGURE 2. (a) The interface resembles a slipper bearing with the gentle slope propagating into the water. (b) The high pressure at the front of the wave crest steepens the interface and the low pressure at the back makes the interface less steep. (c) The pressure distribution in the trough drives one eddy in each trough. (After Feng *et al.* 1995.)

experience in which stable lubricated flow occurs only when the flow velocity exceeds some critical value.

In this paper we confine our attention to the direct numerical simulation of axisymmetric core flows. The shape of the interface and the secondary motions which develop in a ‘flying’ core flow are consistent with what we expected (see figure 2).

Less intuitive is the existence of a threshold Reynolds number corresponding to a change in the sign of the pressure force on the core, from suction at Reynolds numbers below the threshold, as in the reversed slipper bearing in which the slipper is sucked to the wall, to compression for Reynolds numbers greater than the threshold as in flying core flow in which the core can be pushed off the wall by stagnation pressure.

2. Governing equations

Consider two concentric immiscible fluids flowing down an infinite horizontal pipeline; the core is occupied by fluid 1 and the annulus by fluid 2. Assume also that the core is axisymmetric with interfacial waves. The waves are periodic along the axis and move at certain uniform speed c . The governing equations are

$$\left. \begin{aligned} \frac{1}{r} \frac{\partial}{\partial r}(ru) + \frac{\partial v}{\partial x} &= 0, \\ \rho_i \left(\frac{\partial u}{\partial t} + u \frac{\partial u}{\partial r} + v \frac{\partial u}{\partial x} \right) &= -\frac{\partial P}{\partial r} + \mu_i \left(\frac{1}{r} \frac{\partial}{\partial r} \left(r \frac{\partial u}{\partial r} \right) + \frac{\partial^2 u}{\partial x^2} - \frac{u}{r^2} \right), \\ \rho_i \left(\frac{\partial v}{\partial t} + u \frac{\partial v}{\partial r} + v \frac{\partial v}{\partial x} \right) &= -\frac{\partial P}{\partial x} + \mu_i \left(\frac{1}{r} \frac{\partial}{\partial r} \left(r \frac{\partial v}{\partial r} \right) + \frac{\partial^2 v}{\partial x^2} \right), \end{aligned} \right\} \quad (2.1)$$

where (u, v) are the radial and axial velocity, and

$$P = -\beta x + p(r, x, t) + C_0(t) \quad (2.2)$$

is the pressure, β is the driving pressure gradient, (μ_i, ρ_i) are the viscosity and density in the core $i = 1$ and annulus $i = 2$. We seek a periodic solution in which the time t enters only as $x - ct$ in a wave which propagates with a constant speed c . Then, we can express the condition that the motion be periodic with period L in x as follows:

$$\left. \begin{aligned} u &= u(x - ct, r) = u(x + L - ct, r), \\ v &= v(x - ct, r) = v(x + L - ct, r), \\ p(x - ct, r) &= p(x + L - ct, r). \end{aligned} \right\} \quad (2.3)$$

We next introduce new variables

$$z = x - ct \quad (2.4)$$

and

$$\left. \begin{aligned} w(z, r) &= v(x - ct, r) - c, \\ u(z, r) &= u(x - ct, r), \\ P(z, r) &= P(x - ct, r) = -\beta(z + ct) + p(r, z) + C_0(t). \end{aligned} \right\} \quad (2.5)$$

The system of equations arising from (2.1), (2.4) and (2.5) is to be time independent

$$C_0(t) - \beta ct = C_{pi},$$

where C_{pi} is constant. In these new variables, z replaces x in (2.1) and

$$\left. \begin{aligned} \frac{1}{r} \frac{\partial}{\partial r} (ru) + \frac{\partial w}{\partial z} &= 0, \\ \rho_i \left(u \frac{\partial u}{\partial r} + w \frac{\partial w}{\partial z} \right) &= -\frac{\partial p}{\partial r} + \mu_i \left(\frac{1}{r} \frac{\partial}{\partial r} \left(r \frac{\partial u}{\partial r} \right) + \frac{\partial^2 u}{\partial z^2} - \frac{u}{r^2} \right), \\ \rho_i \left(u \frac{\partial w}{\partial r} + w \frac{\partial w}{\partial z} \right) &= \beta - \frac{\partial p}{\partial z} + \mu_i \left(\frac{1}{r} \frac{\partial}{\partial r} \left(r \frac{\partial w}{\partial r} \right) + \frac{\partial^2 w}{\partial z^2} \right). \end{aligned} \right\} \quad (2.6)$$

At the pipe wall $r = R_2$

$$u = 0, \quad w = -c, \quad (2.7)$$

and at the centre of the core $r = 0$, we require

$$u = 0, \quad \frac{\partial w}{\partial z} = 0. \quad (2.8)$$

The interface is given by

$$r = f(z) = f(z + L). \quad (2.9)$$

Here, between the water and oil, the kinematics condition is

$$u = \frac{df}{dt} = \frac{\partial f}{\partial t} + v \frac{\partial f}{\partial x} = w \frac{\partial f}{\partial z}, \quad (2.10)$$

and the velocity condition is $[\hat{U}] = 0$, where $[\cdot] = (\cdot)_1 - (\cdot)_2$ and

$$\hat{U} = (u, w). \quad (2.11)$$

The normal stress condition is

$$(-[P] + 2H\sigma) + \mathbf{n} \cdot [2\mu \mathbf{D}[\hat{U}]] \cdot \mathbf{n} = 0, \quad (2.12)$$

and the shear stress condition is

$$\mathbf{t} \cdot [2\mu \mathbf{D}[\hat{U}]] \cdot \mathbf{n} = 0, \quad (2.13)$$

where $D[\hat{U}] = \frac{1}{2}(\nabla\hat{U} + \nabla\hat{U}^T)$, $2H$ is the sum of the principal curvatures, σ is the coefficient of interfacial tension, $\mathbf{n} = \mathbf{n}_{12}$ is the normal from liquid 1 to 2 and \mathbf{t} is the tangent vector.

In addition, we prescribe the oil flow rate

$$Q_0 = \frac{1}{L} \int_0^L \left\{ \int_0^f 2\pi r v(r, z) dr \right\} dz, \quad (2.14)$$

and water flow rate

$$Q_w = \frac{1}{L} \int_0^L \left\{ \int_f^{R_2} 2\pi r v(r, z) dr \right\} dz. \quad (2.15)$$

3. Rigid deformable core flow

In many situations, the viscosity of the oil is much greater than the viscosity of water. In this case the flow of the oil can be varied as a superposition of creeping motions on the forward motion of a rigid core. The surpassingly slow secondary motions should not have a sensible effect on the overall dynamics. We shall therefore assume that the core is solid with standing waves on the interface. A consequence of the assumption is that non-rigid motions of the core may be neglected. In this rigid deformable core model, the core is stationary ($\hat{U}_1 = 0$) and water moves. The velocity for wavy core flow can be written (figure 3) as

$$\hat{U} = u\mathbf{e}_r + w\mathbf{e}_z = U_n \mathbf{n} + U_s \mathbf{t}, \quad (3.1)$$

where U_n is the normal component and U_s is the tangential component of the velocity on the interface $r = f(z)$.

The continuity of the shear stress gives rise to

$$\frac{\partial U_{s1}}{\partial n} = \frac{\mu_2}{\mu_1} \frac{\partial U_{s2}}{\partial n} = m \frac{\partial U_{s2}}{\partial n}. \quad (3.2)$$

So, no matter what the value of

$$\frac{\partial U_{s2}}{\partial n} = O(1) \quad \text{is} \quad \frac{\partial U_{s1}}{\partial n} \sim O(m).$$

For heavy crudes in water $m = \mu_2/\mu_1 = O(10^{-5})$ is very small, compatible with the assumption that \hat{U}_1 is effectively zero.

From continuity of velocity on the interface, $[[\hat{U}]] = 0$, we also find that the water velocity is zero on the interface. Since the relative velocity in the solid core vanishes, the speed c of the advected wave, in coordinates in which the wall is stationary, is exactly the core velocity $c = w(r, z)$ which is constant, independent of r and z when $r \leq f(z)$. In this case (2.14) reduces to

$$Q_0 = \pi R_1^2 c, \quad (3.3)$$

and

$$R_1^2 = \frac{1}{L} \int_0^L f^2(z) dz. \quad (3.4)$$

The viscous part of the normal stress on the interface vanishes:

$$\mathbf{n} \cdot [[2\mu D[\hat{U}]]] \cdot \mathbf{n} = 2\mu_1 \frac{\partial U_{n1}}{\partial n} - 2\mu_2 \frac{\partial U_{n2}}{\partial n} = 0, \quad (3.5)$$

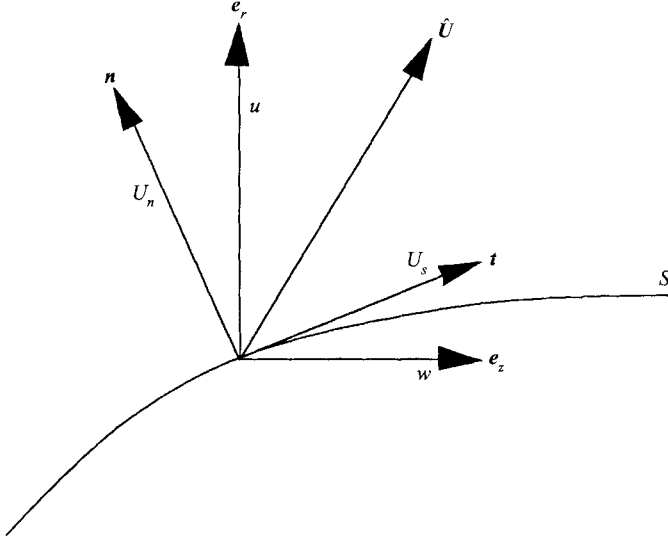


FIGURE 3. The velocity components are in different coordinates.

since

$$\frac{\partial U_s}{\partial s} + \frac{\partial U_n}{\partial n} = 0,$$

and on the interface

$$\frac{\partial U_s}{\partial s} = 0. \quad (3.6)$$

Therefore, the normal stress balance (2.12) reduces to

$$[[P]] = 2H\sigma. \quad (3.7)$$

Apart from the pressure difference required to balance interfacial tension, the pressure in an established flow must be the same on each cross-section. Hence the pressure in the core is

$$P_1 = -\beta z + C_{p1}, \quad (3.8)$$

while the pressure in the annulus is

$$P_2 = -\beta z + p(r, z) + C_{p2}. \quad (3.9)$$

Since the pressure level is indeterminate we may, without loss of generality, put

$$C_{p2} = 0. \quad (3.10)$$

In the water, $f \leq r \leq R_2$, we have

$$\left. \begin{aligned} \frac{1}{r} \frac{\partial}{\partial r} (ru) + \frac{\partial w}{\partial z} &= 0, \\ \rho_2 \left(u \frac{\partial u}{\partial r} + w \frac{\partial u}{\partial z} \right) &= -\frac{\partial p}{\partial r} + \mu_2 \left(\frac{1}{r} \frac{\partial}{\partial r} \left(r \frac{\partial u}{\partial r} \right) + \frac{\partial^2 u}{\partial z^2} - \frac{u}{r^2} \right), \\ \rho_2 \left(u \frac{\partial w}{\partial r} + w \frac{\partial w}{\partial z} \right) &= \beta - \frac{\partial p}{\partial z} + \mu_2 \left(\frac{1}{r} \frac{\partial}{\partial r} \left(r \frac{\partial w}{\partial r} \right) + \frac{\partial^2 w}{\partial z^2} \right). \end{aligned} \right\} \quad (3.11)$$

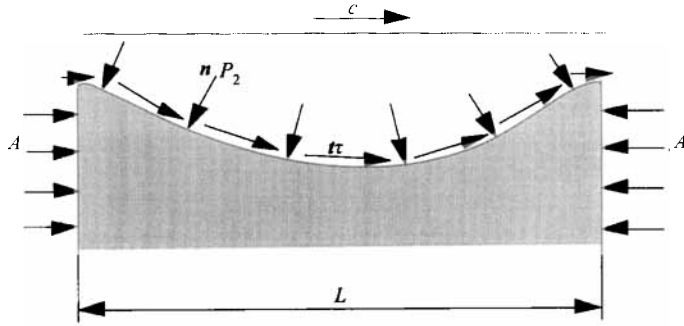


FIGURE 4. Force balance on the wave core is based on one wavelength. The pressure drop is βL and $A\beta L = F_z$ is the force.

And in the oil core, $0 < r < f$

$$\frac{dP_1}{dz} = -\beta. \quad (3.12)$$

The normal stress balance at $r = f$ which is given by (3.8), then becomes

$$\frac{\sigma}{f \left(1 + \left(\frac{df}{dz} \right)^2 \right)^{1/2}} - \frac{\sigma \frac{d^2 f}{dz^2}}{\left(1 + \left(\frac{df}{dz} \right)^2 \right)^{3/2}} = [P] = P_1 - P_2 = C - p. \quad (3.13)$$

To solve our problem we must prescribe β , and compute c , or we may give c and compute β . Since the momentum change in one wavelength is zero, we may relate c and β by the force balance shown in figure 4 and expressed as

$$\begin{aligned} A\beta L = F_z &= 2\pi \int_0^{S_L} f(\mathbf{n}P_2 + \mathbf{t}\tau) \cdot \mathbf{e}_z ds = 2\pi \int_0^L (\mathbf{n}P_2 + \mathbf{t}\tau) \cdot \mathbf{e}_z f(1 + (df/dz)^2)^{1/2} dz, \\ &= 2\pi \int_0^L (P_2 \sin \theta + \tau \cos \theta) f(1 + (df/dz)^2)^{1/2} dz \end{aligned} \quad (3.14)$$

where

$$\tan \theta = \frac{df}{dz}, \quad (3.15)$$

and βL is the pressure drop, A is the area of the cross-section of the core, S_L is the arclength in one wavelength $r = f$, \mathbf{n} is the unit normal vector, \mathbf{t} is the unit tangent vector, \mathbf{e}_z is the unit vector in the axial direction, and τ is the shear stress.

The pressure P_2 and shear stress τ depend on c implicitly; we give c and compute P_2 and τ . The corresponding β is given by iteration using (3.14).

We must now solve (3.11) for L periodic functions u , w , p subject to the conditions that $w = -c$, at $r = R_2$, $w = u = 0$ at $r = f(z)$ where Q_w is prescribed by (2.15), the pressure and interfacial tension are related by (3.13) and β and c are related by (3.14). To solve this, we first prescribe the shape $f_0(z)$ of the wave with a prescribed mean R_1 and, of course, its length L_0 and the speed c . We next construct a sequence of iterations in which c , R_1 , and Q_w are fixed. We first compute u , w and p satisfying all the conditions

except (3.13). The pressure p_0 , belonging to $f_0(z)$, then determines a new shape $f_1(z)$ to satisfy (3.13). A certain constant C_1 is required to maintain the value of R_1 in the iteration. At the next stage we repeat the calculation of u_1 , w_1 and p_1 . This gives a new $f_2(z)$ and C_2 , and so on.

We can, therefore, calculate convergent solutions corresponding to each and every triplet (c, R_1, Q_w) . We do not expect all these solutions to be stable. In experiments we obtain one R_1 when we prescribe the inputs Q_w and Q_0 or c . This should be equivalent to prescribing two other independent items of data, say c and R_1 . Then we would expect one Q_w for each c and R_1 to appear in experiments, but we calculate a family of solutions for the given c and R_1 and any Q_w . When the parameters are taken for perfect core flow, we get perfect core flow from our simulation; most of these perfect core flows are actually unstable. Our simulation then can be regarded as giving rise to a one parameter family of wavy core flows whose stability is yet to be tested.

4. The hold-up ratio in wavy core flow

The hold-up ratio h is the ratio Q_0/Q_w of volume flow rates to the ratio V_0/V_w of volume in the pipe:

$$h = \frac{Q_0/Q_w}{V_0/V_w} = \frac{Q_0/Q_w}{R_1^2/(R_2^2 - R_1^2)}, \quad (4.1)$$

The hold-up ratio depends on the fluid properties and flow parameters but is most strongly influenced by flow type. Equation (4.1) can be represented as the ratio of superficial velocities

$$h = \frac{Q_0/\pi R_1^2}{Q_w/\pi(R_2^2 - R_1^2)} = \frac{c_0}{c_w}, \quad (4.2)$$

where

$$c_0 = \frac{Q_0}{\pi R_1^2}, \quad (4.3)$$

$$c_w = \frac{Q_w}{\pi(R_2^2 - R_1^2)}, \quad (4.4)$$

and $c = c_0$ for rigid core flow.

Here, we consider the hold-up ratio in perfect core flow and wavy core flow. A perfect core-annular flow has a perfectly cylindrical interface of uniform radius without waves and is perfectly centred on the pipe axis with an annulus of lubricating water all around. The velocity W and flow rate Q of a perfect core flow is

$$W_0(r) = \frac{\beta}{4\mu_1}(R_1^2 - r^2) + \frac{\beta}{4\mu_2}(R_2^2 - R_1^2), \quad (4.5)$$

$$W_w(r) = \frac{\beta}{4\mu_2}(R_2^2 - r^2), \quad (4.6)$$

$$Q_0 = 2\pi \int_0^{R_1} r W_0 \, dr = 2\pi \left\{ \frac{\beta}{16\mu_1} R_1^4 + \frac{\beta}{8\mu_2} (R_2^2 R_1^2 - R_1^4) \right\}, \quad (4.7)$$

$$Q_w = 2\pi \int_{R_1}^{R_2} r W_w(r) \, dr = 2\pi \left\{ \frac{\beta}{16\mu_2} (R_2^2 - R_1^2)^2 \right\}. \quad (4.8)$$

Equations (4.7) and (4.8) can be written as

$$Q_0 = -\frac{\beta\pi R_1^4}{8\mu_2}(m + 2(a^2 - 1)), \quad (4.9)$$

and

$$Q_w = -\frac{\beta\pi R_1^4}{8\mu_2}(a^2 - 1)^2. \quad (4.10)$$

The ratio of the flow rates, the input ratio, is

$$\gamma = \frac{Q_0}{Q_w} = \frac{m + 2(a^2 - 1)}{(a^2 - 1)^2}, \quad (4.11)$$

where

$$m = \frac{\mu_2}{\mu_1}, \quad a = \frac{R_2}{R_1} = \left(1 + \frac{1}{\gamma}(1 + (1 + m\gamma)^{1/2})\right)^{1/2}.$$

The oil fraction is given by

$$\eta^2 = \left(\frac{R_1}{R_2}\right)^2 = \frac{1}{a^2} = \frac{1}{1 + (1/\gamma)(1 + (1 + m\gamma)^{1/2})}, \quad (4.12)$$

while the water fraction is given by

$$1 - \eta^2 = 1 - \frac{1}{1 + (1/\gamma)(1 + (1 + m\gamma)^{1/2})} = \frac{1 + (1 + m\gamma)^{1/2}}{\gamma + 1 + (1 + m\gamma)^{1/2}}. \quad (4.13)$$

The volume ratio is proportional to the fraction ratio. Hence

$$\frac{V_0}{V_w} = \frac{\eta^2}{1 - \eta^2} = \frac{\gamma}{1 + (1 + m\gamma)^{1/2}}. \quad (4.14)$$

The equation for the hold-up ratio is therefore

$$h = \frac{Q_0/Q_w}{V_0/V_w} = \frac{\gamma}{\frac{\gamma}{1 + (1 + m\gamma)^{1/2}}} = 1 + (1 + m\gamma)^{1/2}. \quad (4.15)$$

For very viscous oil, $m \approx 0$, and $h \approx 2$.

Now let us consider the hold-up ratio for wavy core flow in the system of coordinates in which the wall is stationary. Given a periodic function $f(x - ct) = f(z)$ with wavelength L , the average diameter of the oil core is R_1 , where

$$\frac{1}{L} \int_0^L f^2(z) dz = R_1^2. \quad (4.16)$$

The input rate for a rigid core is related to the wave speed by

$$Q_0 = \pi R_1^2 c = \frac{c\pi}{L} \int_0^L f^2(z) dz \quad (4.17)$$

Since both water and oil flow rates are specified, the total flow rate at each cross-section is constant:

$$Q_{total} = Q_0 + Q_w = \pi f^2(z) c + 2\pi \int_{f(z)}^{R_2} rv(r, z) dr, \quad (4.18)$$

where

$$v(r, z) = \begin{cases} 0, & r = R_2 \\ c, & r = f(z) \end{cases}$$

and the flow inputs Q_0 and Q_w are independent of z . Then, the water input can be written as

$$Q_w = Q_{total} - Q_0 = \pi c[f^2(z) - R_1^2] + 2\pi \int_{f(z)}^{R_2} rv(r, z) dr, \quad (4.19)$$

independent of z .

Equation (4.19) gives an interesting z -dependent decomposition of the constant water input Q_w . We may write (4.19) as

$$Q_w = \Phi(z) + \Psi(z), \quad (4.20)$$

where

$$\Phi = \pi c[f^2(z) - R_1^2] \quad (4.21)$$

and

$$\Psi(z) = 2\pi \int_{f(z)}^{R_2} rv(r, z) dr. \quad (4.22)$$

Suppose that a wave crest at $z = 0$ just touches the pipe wall, $f(z) = R_2$. In this case, the water flow Q_w is entirely due to the forward motion of the water trapped in troughs and

$$\Psi(z) = 0, \quad \Phi(0) = \pi c[R_2^2 - R_1^2],$$

so that $\Phi(z)$ can be said to represent the trapped water. On the other hand, for perfect core flow $\Phi = 0$ for all z .

When Q_0 and Q_w are given, the wave speed c and the average diameter of the oil core depends on the wave shape $f(z)$. The hold-up ratio for wavy core flow is then given by

$$h = \frac{Q_0/Q_w}{R_1^2/(R_2^2 - R_1^2)} = \frac{\pi c R_1^2}{\pi c [f^2 - R_1^2] + 2\pi \int_f^{R_2} rv dr} \frac{R_2^2 - R_1^2}{R_1^2}. \quad (4.23)$$

For perfect core annular flow, the flow rate of trapped water is zero since the core radius is uniform $f^2 = R_1^2$. Using W from (4.8) we get $h = 2$. Let us focus on the flow rates at the cross-section of the wave crest, where $f = f_{max}$ and assume that $f_{max} = R_2$. Then the integral in (4.23) vanishes and the hold-up ratio is 1. Therefore, the hold-up ratio for wavy core flow is between 1 and 2.

In the transition from a perfect core flow to a wavy core flow, the wave troughs will carry extra water even if the average diameter of the oil core is unchanged; this increases the water flow rate. However, when the water flow rate is fixed, the system can not increase the water flow rate. Therefore, the average diameter of the core will increase, reducing the water flow rate. In the wavy flow, more oil is in the pipe than in perfect core flow, and the hold-up ratio is less than 2. Of course, the speed of the core must decrease when there is more oil and oil flow rate is fixed.

The pressure gradient β is related to the difference in area of the core at a crest and average area, this is measured by

$$d = \pi c[f^2(0) - R_1^2]. \quad (4.24)$$

The gap between the pipe wall and wave crest is smaller when d is larger, provided that the volume of oil in the pipe is fixed. Smaller gaps imply high friction and large values of the pressure gradient.

5. Comparison with experiments

Our simulations are for the case in which the density of oil and water are the same; when they are not the same and the pipe is horizontal, the oil core will rise or sink. Some representative wave shapes, which look like those in experiments, are for density matched flows in figure 5.

Bai, Chen & Joseph (1992) carried out experiments and calculated stability results for vertical axisymmetric core flow in the case when the buoyant force and pressure force on the oil are both against gravity (up flow). They observed ‘bamboo’ waves for their oil $\rho_o = 0.905 \text{ g cm}^{-3}$ and $\mu_o = 6.01$ poise in water with $\rho_w = 0.995 \text{ g cm}^{-3}$ and $\mu_w = 0.01$ poise. We have simulated the same flow, with the same parameters except that our core is infinitely viscous. The results show that $\mu_o = 6.01$ is not yet asymptotically infinitely viscous, but nevertheless the agreements are satisfactory.

The equations that we used for our simulation are as follows. In the water, we have

$$\left. \begin{aligned} \frac{1}{r} \frac{\partial}{\partial r}(ru) + \frac{\partial w}{\partial z} &= 0, \\ \rho_2 \left(u \frac{\partial u}{\partial r} + w \frac{\partial u}{\partial z} \right) &= -\frac{\partial p}{\partial r} + \mu_2 \left(\frac{1}{r} \frac{\partial}{\partial r} \left(r \frac{\partial u}{\partial r} \right) + \frac{\partial^2 u}{\partial z^2} - \frac{u}{r^2} \right), \\ \rho_2 \left(u \frac{\partial w}{\partial r} + w \frac{\partial w}{\partial z} \right) &= \beta + \rho_c g - \frac{\partial p}{\partial z} - \rho_2 g + \mu_2 \left(\frac{1}{r} \frac{\partial}{\partial r} \left(r \frac{\partial w}{\partial r} \right) + \frac{\partial^2 w}{\partial z^2} \right). \end{aligned} \right\} \quad (5.1)$$

The pressure in the water is

$$P_2(r, z) = -\beta z + p(r, z) - \rho_c g z + C_2, \quad (5.2)$$

while the pressure in the core is

$$P_1 = -\beta z - \rho_c g z + C_1, \quad (5.3)$$

where g is gravity and ρ_c is the composite density of the mixture

$$\text{and} \quad \left. \begin{aligned} \rho_c &= \rho_1 \eta^2 + (1 - \eta^2) \rho_2, \\ \eta &= \frac{R_1}{R_2}. \end{aligned} \right\} \quad (5.4)$$

We compared wavelengths, wave speeds and waves shapes from our computation with experiments and the linear stability theory in Bai *et al.* (1992). In our comparison, the flow parameters are based on the experimental information, such as flow rates of oil and water, oil volume ratio and hold-up ratio. In Bai *et al.* (1992), the hold-up ratio is a constant 1.39 and the volume ratio of the oil yields the following formula:

$$\frac{R_1^2}{R_2^2} = 1 - \frac{1}{1 + 0.72(Q_o/Q_w)}. \quad (5.5)$$

The results are given in Table 1. In columns I and II, data from Bai *et al.* (1992) were computed by linear theory of stability. In column I, the computations were carried out for the values of Q_o and Q_w prescribed in the experiments. In column II, the calculations were made with the prescribed Q_o and measured value of R_1 corresponding to the observed hold-up ratio $h = 1.39$. The values of η and R corresponding to the given values of Q_o and Q_w for the experiments with $h = 1.39$ and $\sigma = 22.5$ ($J = 11.2 \times 10^4$) are: 1 (0.76, 661), 2 (0.7, 683), 3 (0.61, 722), 4 (0.54, 758), 5 (0.67, 342), 6 (0.74, 328), 7 (0.79, 320), 8 (0.82, 314) and 9 (0.84, 310).

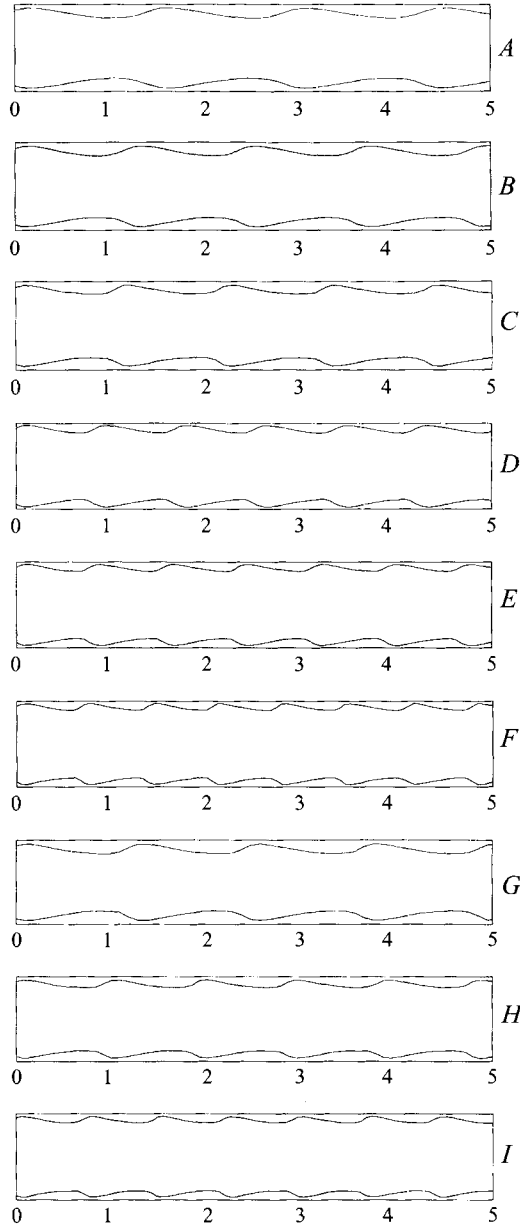


FIGURE 5. Selected wave shapes for water-lubricated axisymmetric flow of oil and water with the same density $\rho = 1.0 \text{ g cm}^{-3}$, $\mu_2 = 0.01$ poise and $\sigma = 26 \text{ dyn cm}^{-1}$ for oil and water. The core is stationary and the wall moves to the right. The pipe diameter is $R_2 = 1.0 \text{ cm}$. Q_0 and Q_w are in $\text{cm}^3 \text{ s}^{-1}$. The data for each frame is given as a triplet of prescribed dimensional value (R_1, Q_0, Q_w) and as a triplet of prescribed dimensionless values $[\eta, h, \mathcal{R}]$ where $\eta = R_1/R_2$, h is the hold-up ratio and Reynolds number \mathcal{R} is defined by (6.8). The dimensionless surface tension $J = 13 \times 10^4$ defined in (6.15) is for all frames. The data for each dimensional and dimensionless triplet are A (0.4, 12.6, 5.05), [0.8, 1.4, 250]; B (0.4, 22.6, 9.09), [0.8, 1.4, 450]; C (0.4, 37.7, 15.2), [0.8, 1.4, 750]; D (0.43, 34.9, 8.8), [0.86, 1.4, 420]; E (0.43, 43.6, 11), [0.86, 1.4, 525]; F (0.43, 69.7, 17.5), [0.86, 1.4, 840]; G (0.39, 26.1, 12), [0.78, 1.4, 600]; H (0.41, 35.2, 12.3), [0.82, 1.4, 600]; I (0.425, 45.4, 12.5), [0.85, 1.4, 600]. Frames A–F show that the wavefront steepens and the wavelength decreases for increasing \mathcal{R} (cf. figure 9). Frames G–I show how the wavelength shrinks as the thickness of the water layer decreases. The wave shape does not change much as η is increased for given values of h and \mathcal{R} because the wavelength and amplitude both decrease. This gives rise to a nearly ‘self-similar’ wave shape leading to ‘sharkskin’ as $\eta \rightarrow 1$ (cf. figure 15).

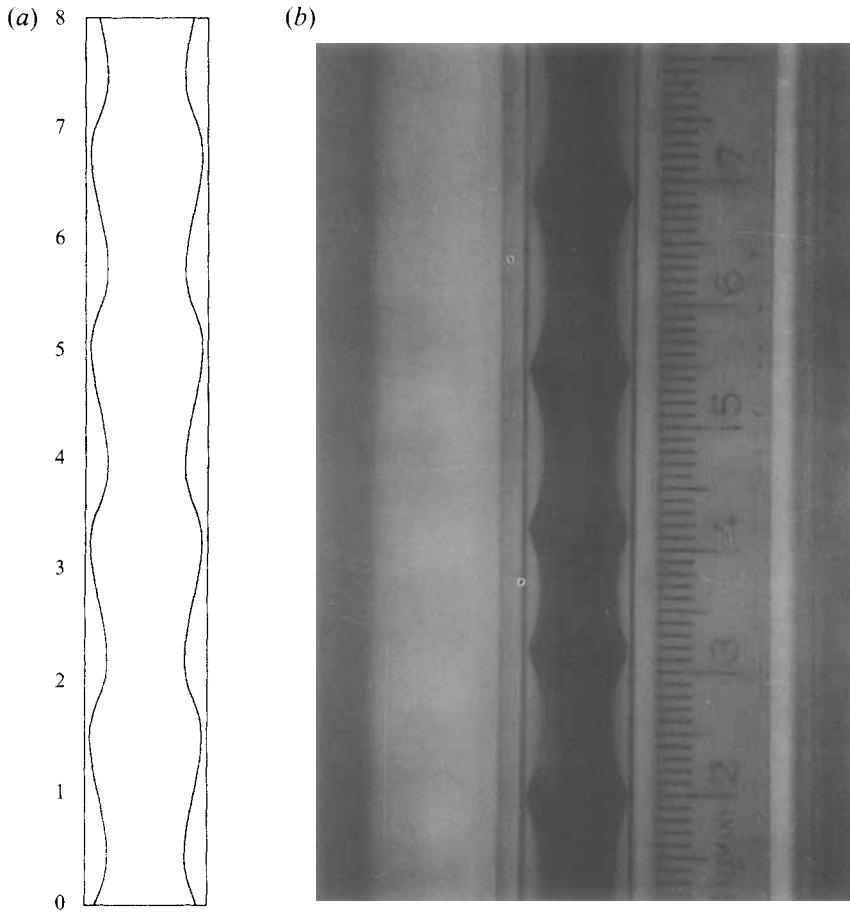


FIGURE 6. (a) Computed waves and (b) bamboo waves, when $[Q_w, Q_0] = [200, 429] \text{ cm}^3 \text{ min}^{-1}$.

No.	Input flowrate		Computations		Experiments		I		II	
	Q_0	Q_w	L (cm)	c (cm s ⁻¹)	L (cm)	c (cm s ⁻¹)	L (cm)	c (cm s ⁻¹)	L (cm)	c (cm s ⁻¹)
1	25.38	13.17	1.32	55.59	1.21	57.7	0.82	79.84	0.79	52.02
2	18.19	13.17	1.66	46.45	1.31	43.28	0.92	80.21	0.96	42.54
3	11.01	13.17	1.70	37.30	1.41	35.65	1.22	79.76	1.22	33.51
4	7.42	13.17	1.33	32.73	1.22	27.81	1.65	77.00	1.33	29.42
5	7.42	6.46	1.77	20.88	1.374	19.16	1.56	58.91	1.25	17.94
6	11.01	6.46	1.66	25.45	1.79	22.90	1.23	58.12	1.16	22.17
7	14.60	6.46	1.39	30.02	1.34	28.22	1.05	54.80	1.02	26.68
8	18.19	6.46	1.15	34.59	1.17	31.06	0.95	50.85	0.87	31.33
9	21.78	6.46	0.96	39.17	0.90	36.25	0.86	49.38	0.79	35.71

TABLE 1. Comparison of computed and measured values of the wave speed c and wavelength L with the linear theory of stability.

The comparison of computed and measured values of the wave speed and wavelength of bamboo waves is given in Table 1. The computed values are slightly larger than the measured values, owing to the fact that motion in the core is neglected with better agreement for faster flow.

Computed wave shapes and the observed shapes of bamboo waves are compared in figures 6–8. The pictures were taken in a vertical pipeline with motor oil ($\rho_o = 0.905 \text{ g cm}^{-3}$, $\mu_o = 6.01 \text{ poise}$) and water ($\rho_w = 0.995 \text{ g cm}^{-3}$, $\mu_w = 0.01 \text{ poise}$). Both water and oil flow against gravity. The water flow rate is fixed at $200 \text{ cm}^3 \text{ min}^{-1}$ while oil flow rate is 429, 825 and $1216 \text{ cm}^3 \text{ min}^{-1}$, respectively.

The computed and observed shapes are alike. In fast flow, the velocity in the oil core is small compared with the velocity in the annulus and the oil core can be considered to be a rigid deformable body. In slower flow (figure 6), the flow inside the core is not so much smaller than the flow in the annulus and the stems of the waves are more readily stretched by buoyancy. Even in this case the agreements are satisfactory.

6. Dimensionless equations

Analysis of this simulation is most useful when carried out in terms of dimensionless variables. In the dimensional equations, we used the following parameters:

$$(R_2, R_1, \mu_2, \rho_2, \sigma, Q_0, Q_w).$$

In the dimensionless formulation, the lengths are scaled with the pipe radius R_2 , pressures are scaled by $\rho_2 U^2$, and velocities are scaled with U . Therefore

$$u = U\bar{u}, \quad (6.1)$$

$$w = U\bar{w}, \quad (6.2)$$

$$r, z, f, L = R_2 \bar{r}, R_2 \bar{z}, R_2 \bar{f}, R_2 \bar{L}, \quad (6.3)$$

$$R_1^2 = \frac{1}{L} \int_0^L f^2 dz = \frac{R_2^2}{\bar{L}} \int_0^{\bar{L}} \bar{f}^2 d\bar{z}, \quad (6.4)$$

$$\eta^2 = \frac{R_1^2}{R_2^2} = \frac{1}{\bar{L}} \int_0^{\bar{L}} \bar{f}^2 d\bar{z}. \quad (6.5)$$

Then (3.11) becomes

$$\left. \begin{aligned} \frac{1}{\bar{r}} \frac{\partial}{\partial \bar{r}} (\bar{r}\bar{u}) + \frac{\partial \bar{w}}{\partial \bar{z}} &= 0, \\ \bar{u} \frac{\partial \bar{u}}{\partial \bar{r}} + \bar{w} \frac{\partial \bar{u}}{\partial \bar{z}} &= -\frac{\partial \bar{p}}{\partial \bar{r}} + \frac{1}{\hat{\mathcal{R}}} \left(\frac{1}{\bar{r}} \frac{\partial}{\partial \bar{r}} \left(\bar{r} \frac{\partial \bar{u}}{\partial \bar{r}} \right) + \frac{\partial^2 \bar{u}}{\partial \bar{z}^2} - \frac{\bar{u}}{\bar{r}^2} \right), \\ \bar{u} \frac{\partial \bar{w}}{\partial \bar{r}} + \bar{w} \frac{\partial \bar{w}}{\partial \bar{z}} &= \bar{\beta} - \frac{\partial \bar{p}}{\partial \bar{z}} + \frac{1}{\hat{\mathcal{R}}} \left(\frac{1}{\bar{r}} \frac{\partial}{\partial \bar{r}} \left(\bar{r} \frac{\partial \bar{w}}{\partial \bar{r}} \right) + \frac{\partial^2 \bar{w}}{\partial \bar{z}^2} \right), \end{aligned} \right\} \quad (6.6)$$

where

$$\hat{\mathcal{R}} = \frac{\rho_2 R_2 U}{\mu_2}. \quad (6.7)$$

We prefer the Reynolds number

$$\mathcal{R} \stackrel{def}{=} \frac{\rho_2 (R_2 - R_1) c}{\mu_2}, \quad (6.8)$$

hence, the relationship between U and c is

$$c = \frac{UR_2}{(R_2 - R_1)} = \frac{U}{1 - \eta}, \quad (6.9)$$

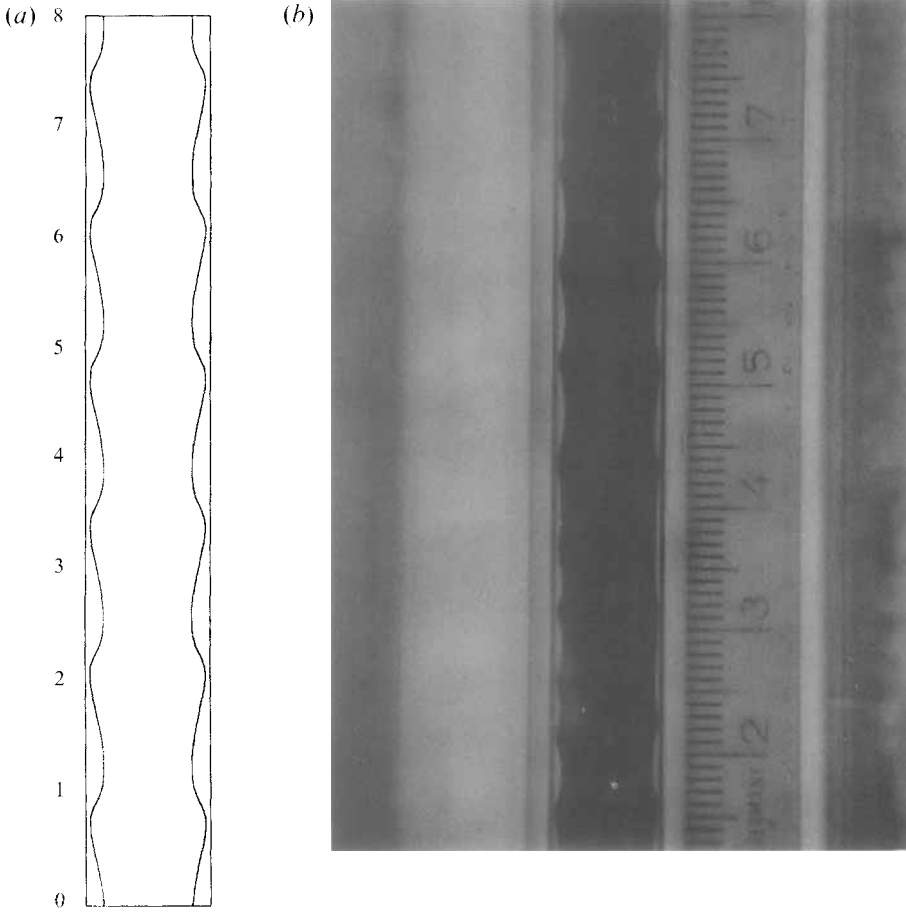


FIGURE 7. (a) Computed waves and (b) bamboo waves, when $[Q_c, Q_a] = [200, 825] \text{ cm}^3 \text{ min}^{-1}$.

and a dimensionless wall speed is

$$\bar{c} = \frac{c}{U} = \frac{1}{1-\eta}. \tag{6.10}$$

At the boundary

$$\bar{u} = \bar{w} = 0 \quad \text{at} \quad r = \bar{f}. \tag{6.11}$$

$$\bar{u} = 0, \quad \bar{w} = \frac{1}{1-\eta} \quad \text{at} \quad \bar{r} = 1. \tag{6.12}$$

The normal stress balance equation becomes

$$\llbracket \bar{P} \rrbracket = \frac{S}{\left(1 + \left(\frac{d\bar{f}}{d\bar{z}}\right)^2\right)^{1/2}} - \frac{S \frac{d^2 \bar{f}}{d\bar{z}^2}}{\left(1 + \left(\frac{d\bar{f}}{d\bar{z}}\right)^2\right)^{3/2}}, \tag{6.13}$$

where

$$S = \frac{\sigma}{\rho_2 U^2 R_2} = \frac{J}{\bar{R}^2}, \tag{6.14}$$

and

$$J = \frac{\rho_2 R_2 \sigma}{\mu_2^2}. \tag{6.15}$$

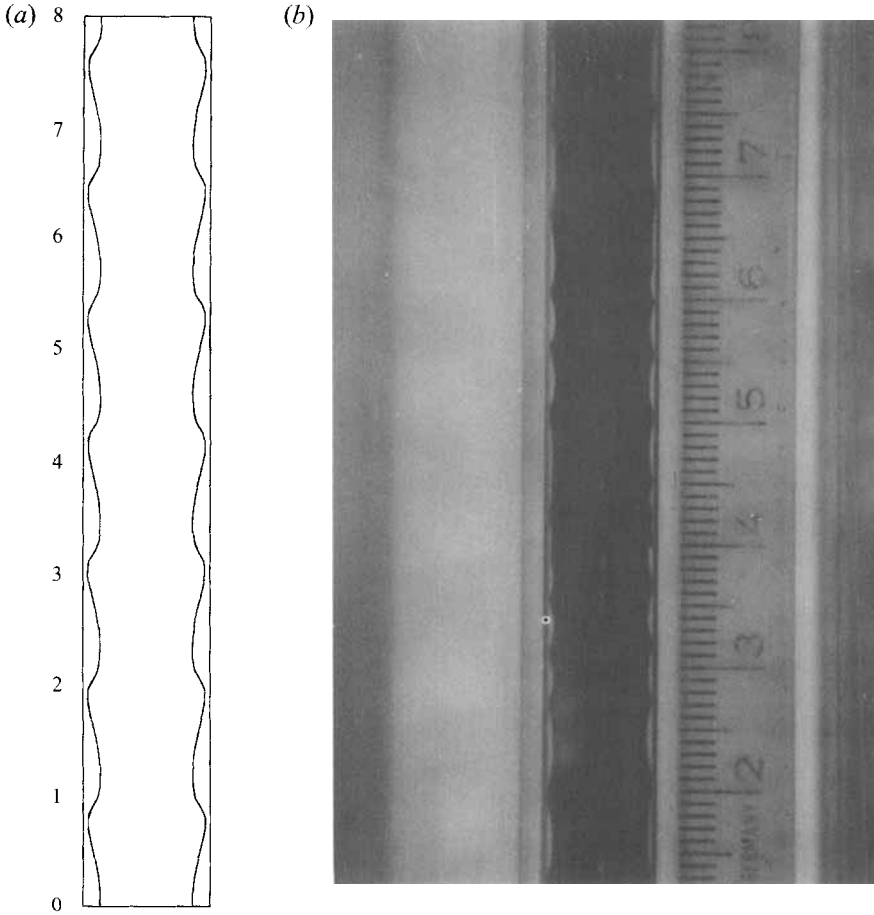


FIGURE 8. (a) Computed waves and (b) bamboo waves, when $[Q_w, Q_0] = [200, 1216] \text{ cm}^3 \text{ min}^{-1}$.

The dimensionless oil flow rate

$$\bar{Q}_0 = \frac{Q_0}{UR_2^2} = \frac{\pi \bar{c}}{L} \int_0^L f^2 dz = \pi \bar{c} \eta^2 = \frac{\pi \eta^2}{1 - \eta}, \quad (6.16)$$

is determined if η is given.

The dimensionless water flow rate may be expressed by the hold-up ratio h using (4.2)

$$\bar{Q}_w = \frac{Q_w}{R_2^2 U} = \frac{1}{R_2^2 U} \int_{R_1}^{R_2} 2\pi r c_w dr = \frac{1}{h} \int_\eta^1 2\pi \bar{c} r dr = \frac{\pi(1 - \eta^2)}{(1 - \eta)h} = \frac{\pi(1 + \eta)}{h}. \quad (6.17)$$

Therefore, only four parameters are required for a complete description of our problem:

$$\mathbb{R}, \eta, J \text{ and } h.$$

All possible problems of scale-up can be solved with this set of parameters.

7. Variation of the flow properties with parameters

Now we shall show how wavelength, pressure gradients, pressure distributions on the interface and wave shape vary with \mathbb{R}, η, h, J .

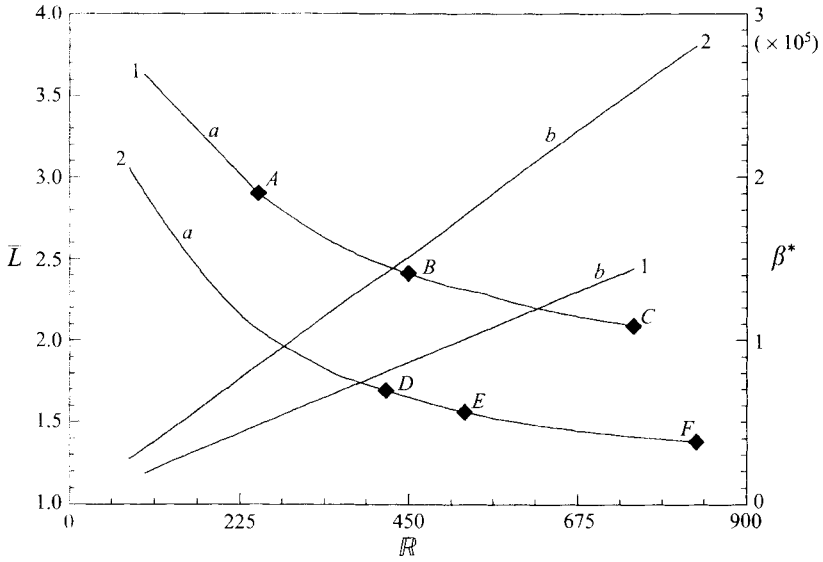


FIGURE 9. (a) Dimensionless wavelength \bar{L} vs. Reynolds number R (6.8) for 1 $[\eta, h, J] = [0.8, 1.4, 13 \times 10^4]$ and for 2 $[\eta, h, J] = [0.86, 1.4, 13 \times 10^4]$; (b) Pressure gradient β^* vs. R under the same conditions. The wave shapes for the points A-F are shown in figure 5.

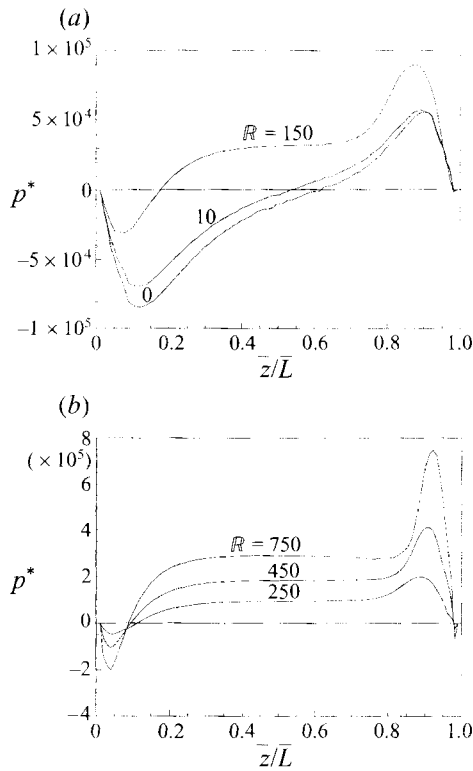


FIGURE 10. (a) Pressure distributions on the interface $p^*(z/\bar{L})$ for $R = 0, 10, 150$ when $[\eta, h, J] = [0.8, 1.4, 13 \times 10^4]$. Note that the pressure force, the area under the pressure curve, is negative for $R = 0, 10$ and is positive when $R = 150$. (b) Pressure distributions on the interface for $R = 250, 450, 750$ when $[\eta, h, J] = [0.8, 1.4, 13 \times 10^4]$. All the pressure forces are positive with the greatest pressure at the forward points of stagnation.

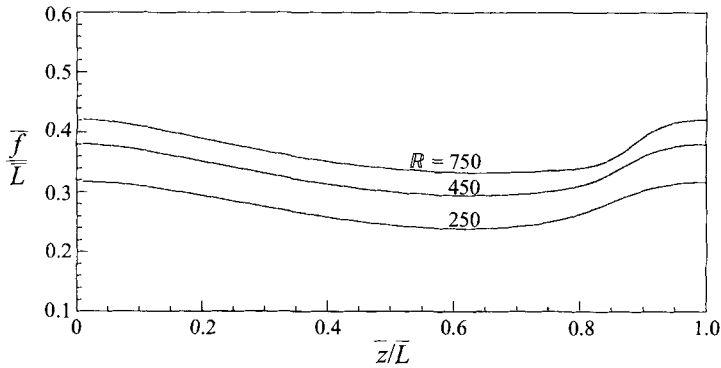


FIGURE 11. Wave shape (\bar{f}/\bar{L} vs. \bar{z}/\bar{L}) for three $R = 250, 450, 750$ when $[\eta, h, J] = [0.8, 1.4, 13 \times 10^4]$.

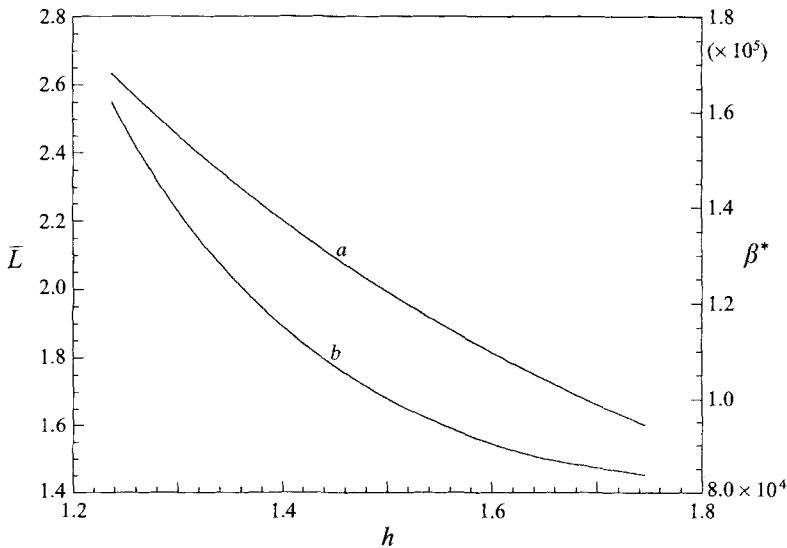


FIGURE 12. (a) Wavelength \bar{L} vs. h for $[\eta, R, J] = [0.8, 600, 13 \times 10^4]$; (b) pressure gradient β^* vs. h under the same conditions.

We have already established that for a highly viscous core in which the oil moves as a rigid body, the hold-up ratio varies between $h = 2$ for perfect core flow and $h = 1$ for the ‘waviest’ possible core flow. In experiments, a unique h is selected when the flow inputs are prescribed so that all but one of the family of solutions for $1 < h < 2$ are apparently unstable. The stable flow selects a certain $h = \tilde{h}$ and a certain wavelength $\tilde{L} = L(Q_0, Q_w, \tilde{h})$. This wavelength appears to be associated to a degree with the length of wave that leads to the maximum rate of growth of small disturbances perturbing perfect core–annular flow (see table 1). The hold-up ratio for the bamboo waves which appear in up-flow in the vertical pipeline studied in the experiments of Bai *et al.* (1992) was about 1.39, independent of the inputs Q_w and Q_0 , and the same $h = 1.39$ is attained in down-flow at large Reynolds numbers. These observations have motivated us to compute many results for $h = 1.4$.

In our computation we chose $J = 13 \times 10^4$ corresponding to the actual physical parameters in wavy core flow in water in which $\mu_2 = 0.01$ poise $\rho = 1 \text{ g cm}^{-3}$, $\sigma =$

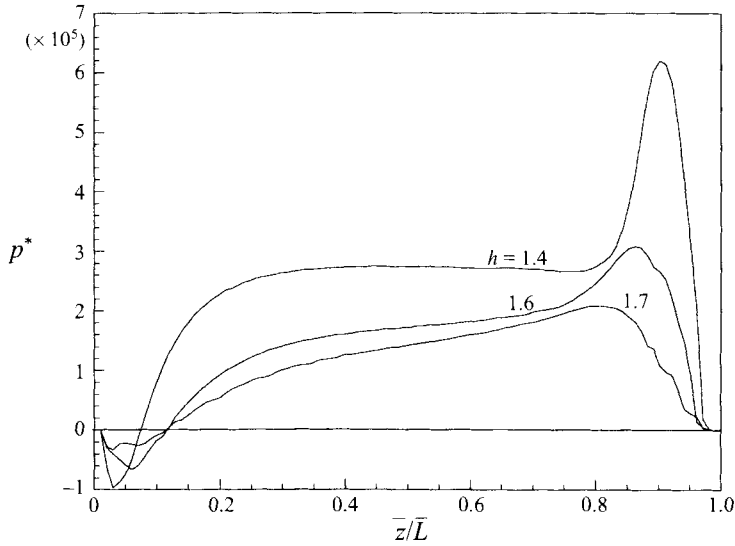


FIGURE 13. Pressure distributions on the interface for different h when $[\eta, \mathcal{R}, J] = [0.8, 600, 13 \times 10^4]$.

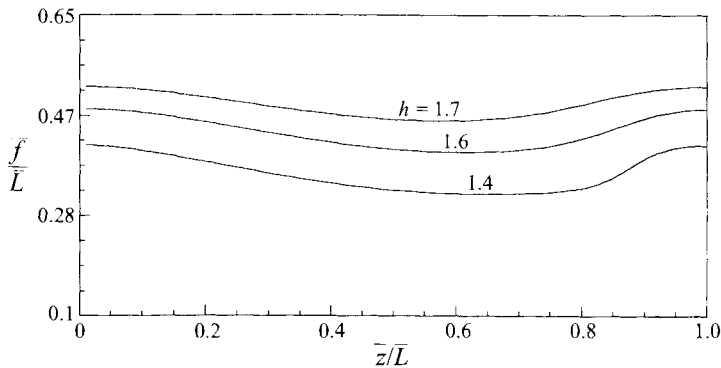


FIGURE 14. Wave shape \bar{f}/\bar{L} vs. \bar{z}/\bar{L} under the conditions specified in figure 13.

26 dyn cm^{-1} , in a pipe of a 1 cm diameter. A value of $\eta = 0.8$ is fairly typical of experiments. The definition of the dimensionless parameter p^* and gradient β^* are

$$p^* = \frac{p(f(z), z) - P_2(f(0), 0)}{\mu^2} \rho R_2^2, \quad (7.1)$$

$$\beta^* = \frac{\rho R_2^2}{\mu^2} \beta. \quad (7.2)$$

The overall pressure is such as to make $p^* = 0$ at the crest of the wave.

Figure 9 shows that the wavelength decreases with \mathcal{R} and the pressure gradient increases linearly with \mathcal{R} for fixed values of η , h and J .

Figures 10 and 11 show that the wave steepens at the front and relaxes at the back of a wave crest as the Reynolds number is increased. The steepening is produced by the high pressures at the stagnation point on the wavefront (of figure 24). The pressure at the stagnation point is probably quadratic in a typical speed on the dividing streamline

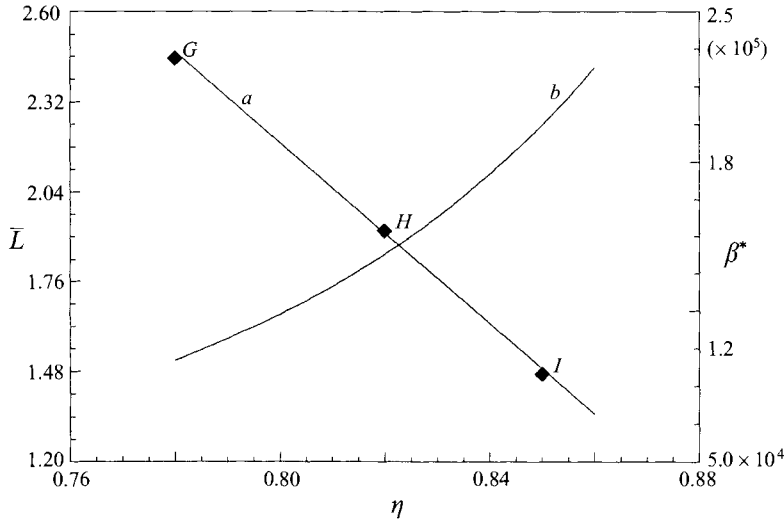


FIGURE 15. (a) Wavelength $\bar{L}(\eta) \approx 13.463 - 14.087\eta$ for $[\mathcal{R}, h, J] = [600, 1.4, 13 \times 10^4]$; (b) pressure gradient β^* vs. η under the same conditions. The wave shapes for the points G, H and I are shown in figure 5. The curve a extrapolates to zero \bar{L} with a finite η . We could not get convergent results for η very close to 1. The extrapolation suggests a limiting zero value of wavelength and amplitude leading to ‘sharkskin’.

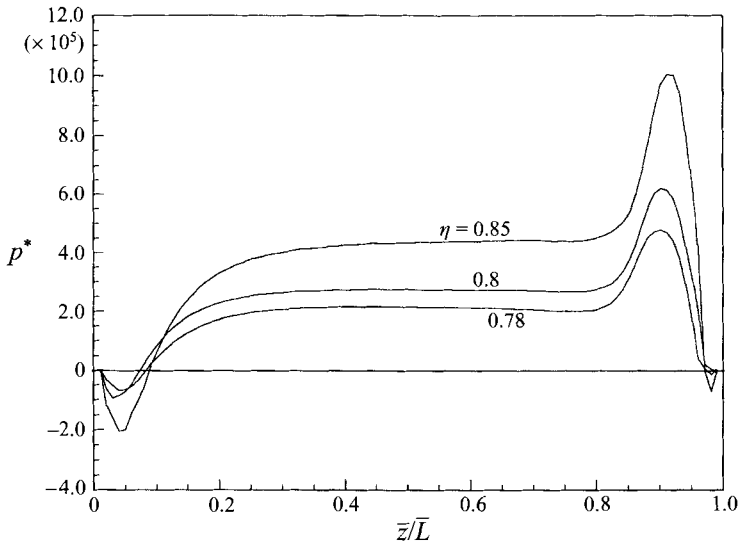


FIGURE 16. Pressure distributions on the interface for different η when $[\mathcal{R}, h, J] = [600, 1.4, 13 \times 10^4]$.

but is not quadratic in the core speed. The pressure force, the area under the pressure curve, changes sign for $10 < \mathcal{R} < 150$. The variation of the pressure force and pressure peak with \mathcal{R} is very nearly linear. This shows that lubrication effects control the pressure even when the wave shape has been strongly distorted by inertia. This situation is similar to the case of levitation of a low-flying elliptical capsule studied by Feng *et al.* (1995).

Figures 12, 13 and 14 show how the wavelength, the pressure gradient, pressure

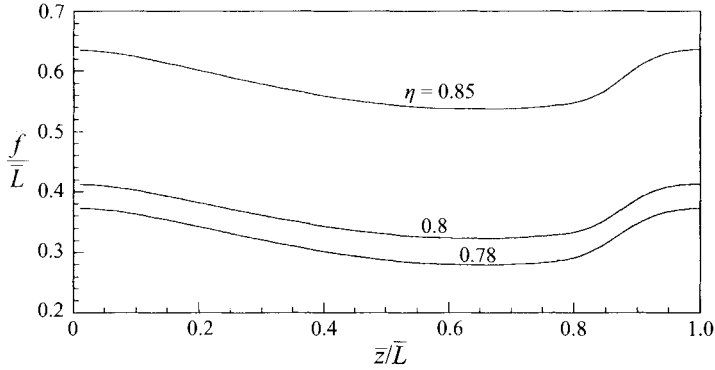


FIGURE 17. Wave shapes for the conditions of figure 16.

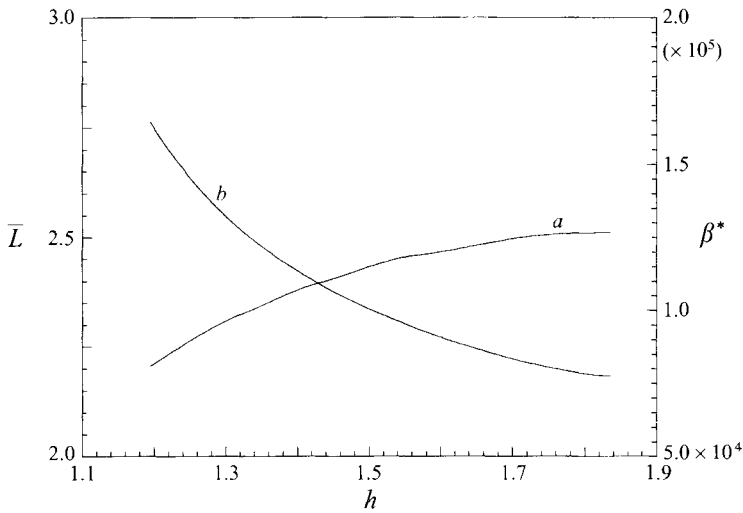


FIGURE 18. (a) Wavelength \bar{L} vs. h for $[\eta, R, J] = [0.8, 0, 13 \times 10^4]$; (b) pressure gradient β^* vs. h under the same conditions.

distribution and waveforms vary with h when $[\eta, R, J] = [0.8, 600, 13 \times 10^4]$. The wave shape is more unsymmetric and the pressure force is greater when h is close to 1. The wavelength is a decreasing function of h when $R = 600$, but is an increasing function of h when $R = 0$ for the same parameters (cf. figure 20).

Figures 15, 16 and 17 show how the wavelength, the pressure gradient and waveforms vary with η when $[R, h, J] = [600, 1.4, 13 \times 10^4]$. The wavelength decreases and the positive pressure peak and wavefront slope all increase as the gap becomes smaller. This suggests that the levitating pressure force will intensify as the gap becomes smaller when the density of the oil and water are different. Moreover, figure 15 shows that $\bar{L}(\eta) \approx a - b\eta$ so that the wavelength $\bar{L}(\eta)$ apparently tends to zero as $\eta \rightarrow 1$ (cf. figure 15). The wave shape is nearly ‘self similar’ in this limit leading to ‘sharkskin’.

Figures 18, 19 and 20 show how the wavelength, the pressure gradient, pressure distribution and waveforms vary with h when $[\eta, R, J] = [0.8, 0, 13 \times 10^4]$. The wave shape is more unsymmetric and the pressure force is greater when h is close to 1. The wavelength is an increasing function of h when $R = 0$.

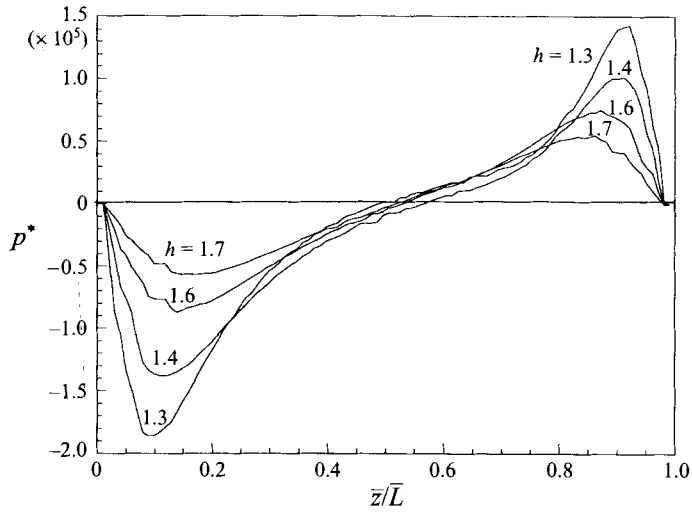


FIGURE 19. Pressure distributions on the interface for different h when $[\eta, \mathcal{R}, J] = [0.8, 0, 13 \times 10^4]$.

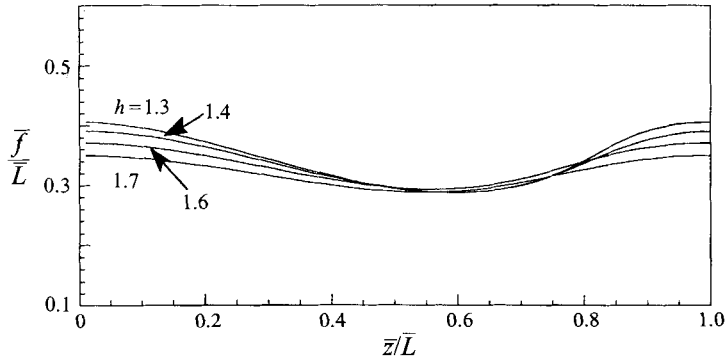


FIGURE 20. Wave shape \bar{f}/\bar{L} vs. \bar{z}/\bar{L} under the conditions specified in figure 19.

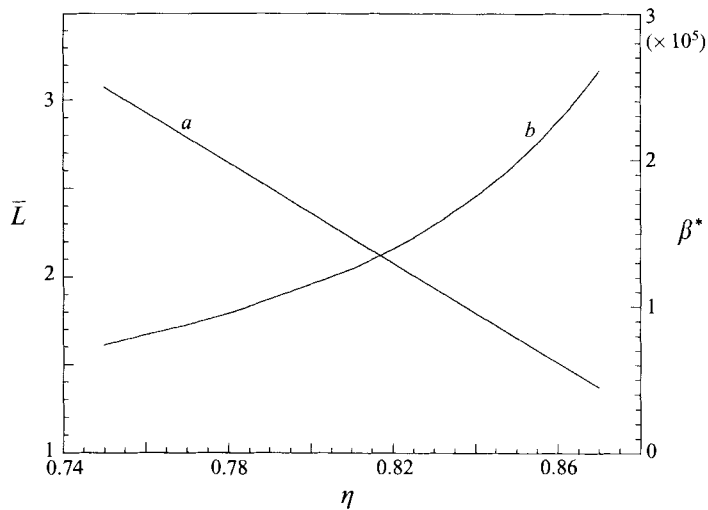


FIGURE 21. (a) Wavelength \bar{L} vs. η for $[\mathcal{R}, h, J] = [0, 1.4, 13 \times 10^4]$; (b) pressure gradient β^* vs. η under the same conditions.

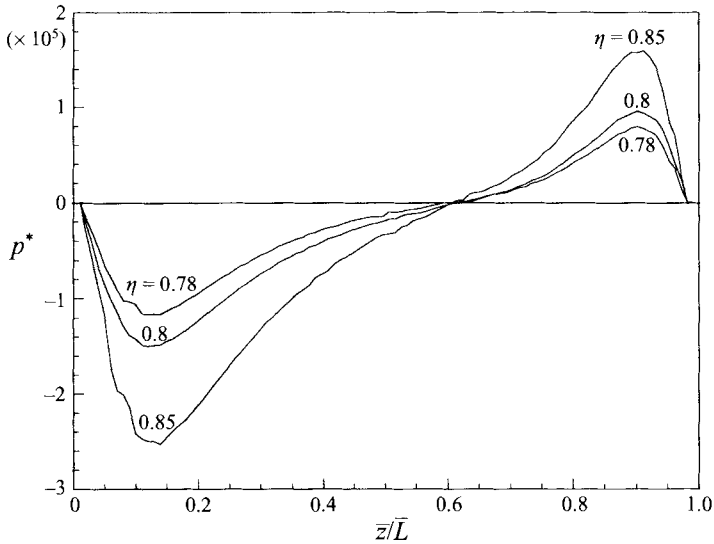


FIGURE 22. Pressure distributions on the interface for different η when $[\mathcal{R}, h, J] = [0, 1.4, 13 \times 10^4]$.

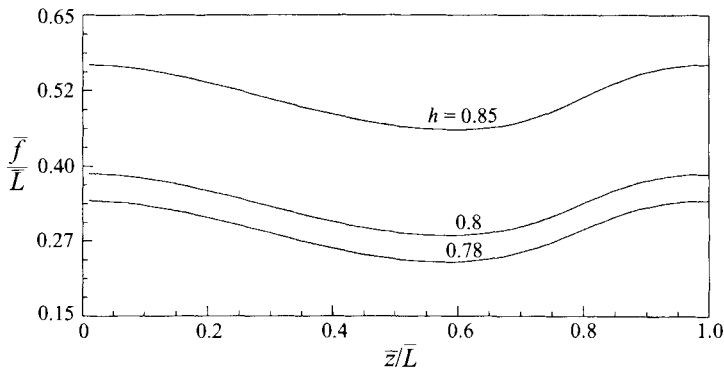


FIGURE 23. Wave shapes for the conditions of figure 22.

Figures 21, 22 and 23 show how the wavelength, the pressure gradient and waveforms vary with η where $[h, \mathcal{R}, J] = [1.4, 0, 13 \times 10^4]$. The pressure force is negative under all conditions, and it is even more negative when gap is small. The waveforms, nevertheless, are steeper on the front than on the rear face, though this asymmetry is less pronounced than at higher Reynolds numbers.

When the flow is driven by pressure, there is friction between the core and the wall which induces a secondary motion most easily seen in a frame moving with the core. Figure 24 shows these secondary motions for $\mathcal{R} = 0$ and $\mathcal{R} = 750$. The pressure distributions are shown in figure 10 for $\mathcal{R} = 0$ and for $\mathcal{R} = 750$. The flow has two parts; a more or less straight flow from left to right and an eddy. There are two points where the flow separates or rejoins the main flow. The high pressure at the front of the crest of the wave propagating into the water appears to be associated with a dividing streamline, while the low pressure at the back of the crest of the wave is related to rejoining the streamline. The pressure is high and positive at the separation point and low and negative at the reattachment point. The waveforms are more symmetric when $\mathcal{R} = 0$ and the pressure variations are moderate with positive pressure on the right at

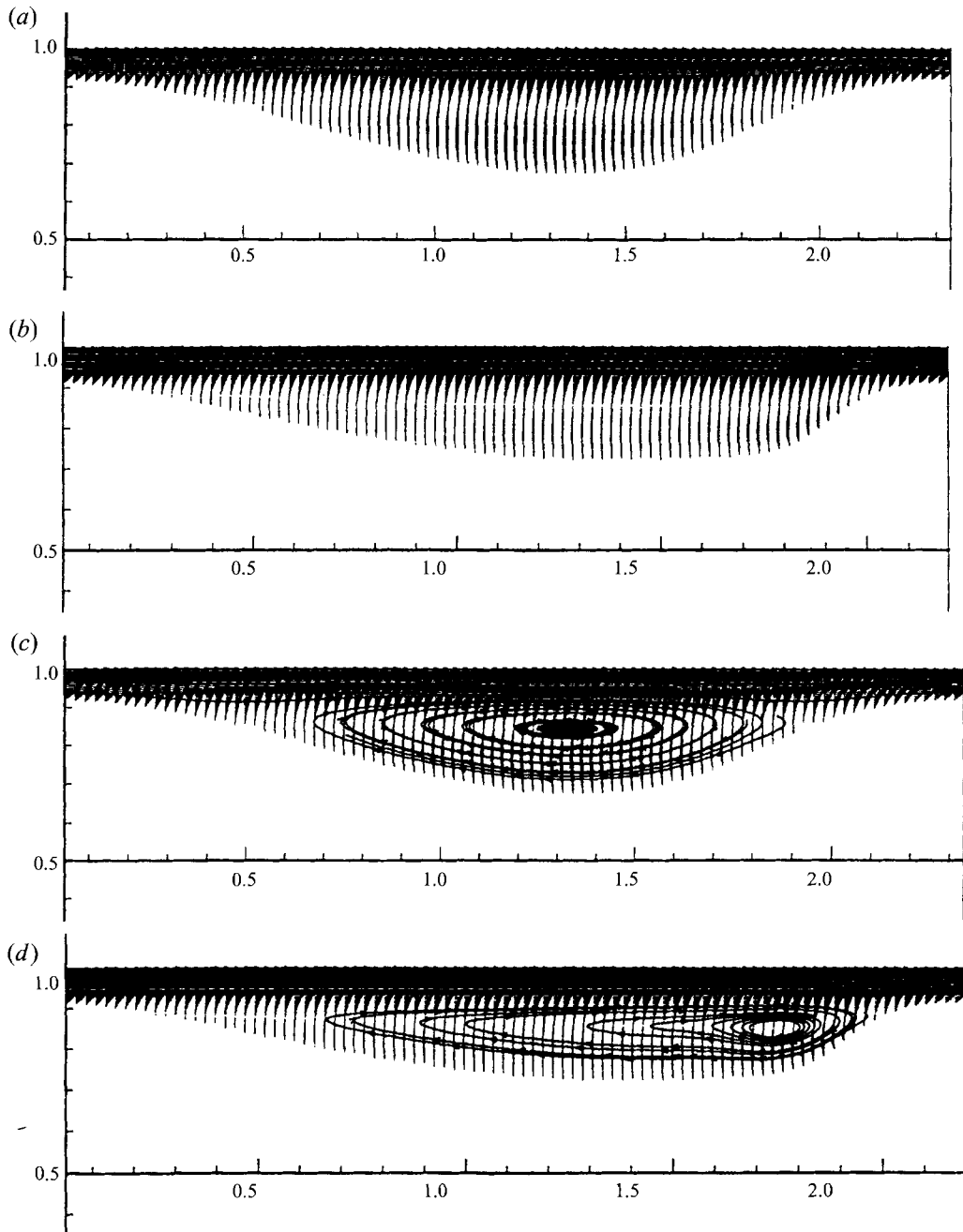


FIGURE 24. Secondary motions for (a) $[\mathcal{R}, \eta, h, J] = [0, 0.8, 1.4, 13 \times 10^4]$, (b) $[\mathcal{R}, \eta, h, J] = [750, 0.8, 1.4, 13 \times 10^4]$; The pressure at the stagnation point on the steep slope at the right corresponds to the pressure maximum shown in figure 10(b), (c) the eddies for Stokes flow as the same condition of (a), (d) the eddies as the same condition of (b).

separation points and slightly larger negative pressures at the left, at reattachment points. Overall, the pressure force for $\mathcal{R} = 0$ is negative and the eddy is more or less centrally located. When $\mathcal{R} = 750$, the waveform, the secondary motion and the pressure distribution are profoundly influenced by inertia. The forward slope of the

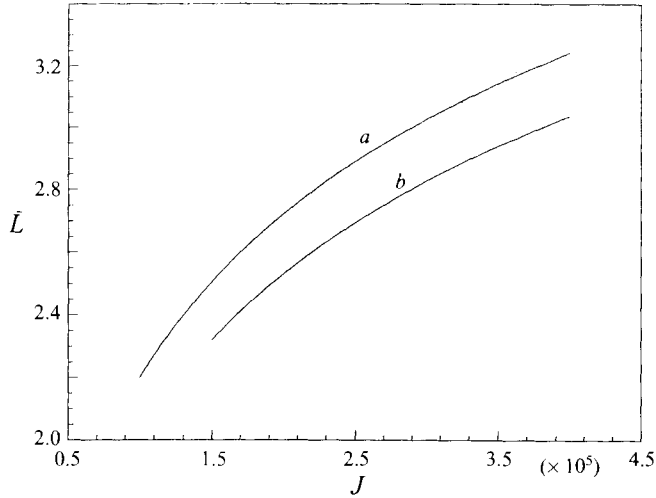


FIGURE 25. Wavelength \bar{L} vs. J , (a) $[\mathcal{R}, \eta, h] = [0, 0.8, 1.4]$; (b) $[\mathcal{R}, \eta, h] = [600, 0.8, 1.4]$.

wave steepens and the rearward slope relaxes, the eddy moves down and to the forward face; the stagnation pressures there grown substantially while the reattachment pressures decline. All this results in a strongly positive pressure force.

Figure 25 shows that the wavelength increases with surface tension, which smooths the wave.

8. Threshold Reynolds numbers and levitation of wavy core flows

The total pressure force on the core is an integral of the pressure on the core surface, the area under the pressure curves shown, say, in figures 10, 13, 16, 19 and 21. The total pressure force is negative at zero and small Reynolds numbers, and is more and more positive as the Reynolds number is increased past a threshold. Figure 26 shows that the wavelength $\bar{L}(h)$ is an increasing function of h when $\mathcal{R} = 0$ and is a decreasing function of h when \mathcal{R} is greater than some threshold.

The concept of a threshold may be formulated in terms of the pressure force

$$F_r = \frac{2\pi}{\bar{L}} \int_0^{S_L} \bar{f} p^* \mathbf{n} \cdot \mathbf{e}_r ds, \tag{8.1}$$

where \mathbf{n} is the normal to the core and S is the arclength. The pressure p^* in (8.1) is chosen to be zero at wave crests. Since the pressure level is not determined by any condition in our problem, our choice is consistent but arbitrary. The radial component $\tau t \cdot \mathbf{e}_r$ of the shear stress vanishes at crests and troughs and at two other points where $\tau = 0$. This term does not make a sensible contribution to the radial force. Figure 27 gives the locus of points where $F_r = 0$, with $F_r < 0$ below and $F_r > 0$ above. The threshold value is always positive though it decreases with h , since $F_r < 0$ for Stokes flow. In figure 28 we plotted F_r for $h = 1.9$ where $\eta = 0.9$. This is a case in which lubrication theory might be used; however, \mathcal{R}_c is about 2.25 so that the pressure force is negative for lubrication theory (see §9). Figure 29 shows that the wavelength changes with hold-up ratio for $[\eta, \mathcal{R}, J] = [0.8, 100, 13 \times 10^4]$. The slope dL/dh is greater than zero in a lower hold-up ratio and less than zero in a higher hold-up ratio.

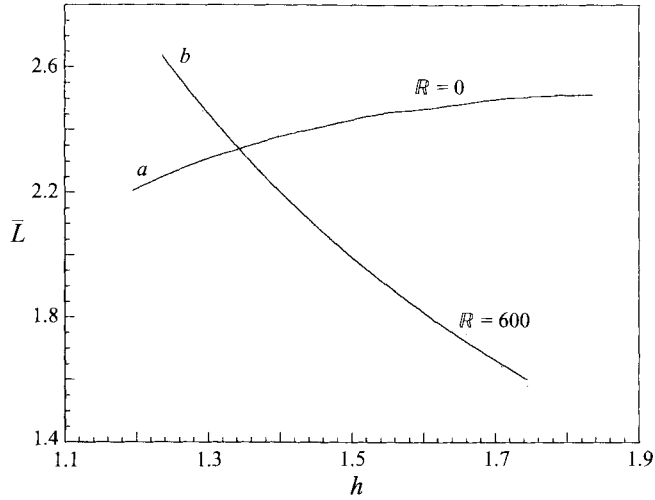


FIGURE 26. Wavelength \bar{L} vs. h , for (a) $[\eta, \mathcal{R}, h] = [0.8, 0, 13 \times 10^4]$, and for (b) $[\eta, \mathcal{R}, J] = [0.8, 600, 13 \times 10^4]$.

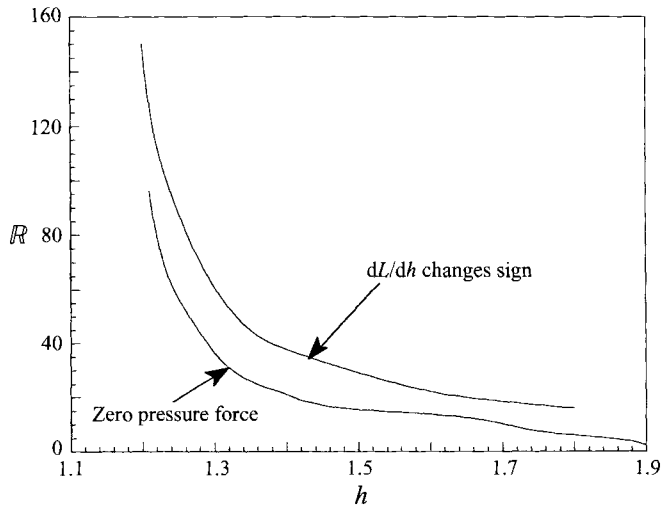


FIGURE 27. Threshold Reynolds numbers \mathcal{R} vs. h for $[\eta, J] = [0.8, 13 \times 10^4]$.

We may argue that a positive levitation of a lighter or a heavier than water core flow requires a positive pressure force to push the core away from wall. The pressure forces are associated with the form of waves that they generate. Waves also develop in Stokes flow, but the pressure forces associated with these waves are negative like those on the reversed slipper bearing which pull the slipper to the wall. When the Reynolds number is higher than the threshold, high positive pressures are generated, especially at the stagnation point on the steep part of the wavefront (figure 24).

In the axisymmetric problem with matched density considered here, lateral motions of the core off centre are not generated by pressure forces, whether they be positive or negative, because the same pressure acts all around the core. We may consider what might happen if the core moved to a slightly eccentric position owing to a small difference in density. The pressure distribution in the narrow part of the gap would intensify and the pressure in the wide part of the gap would relax according to the

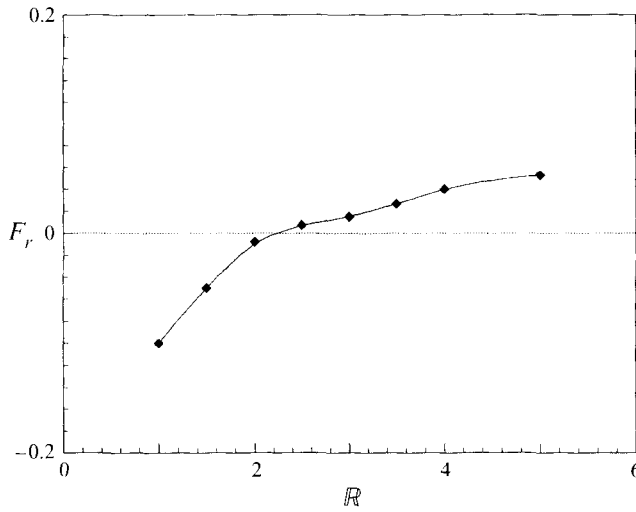


FIGURE 28. Pressure force due to pressure on the interface vs. R for $[\eta, h, J] = [0.9, 1.9, 13 \times 10^4]$.

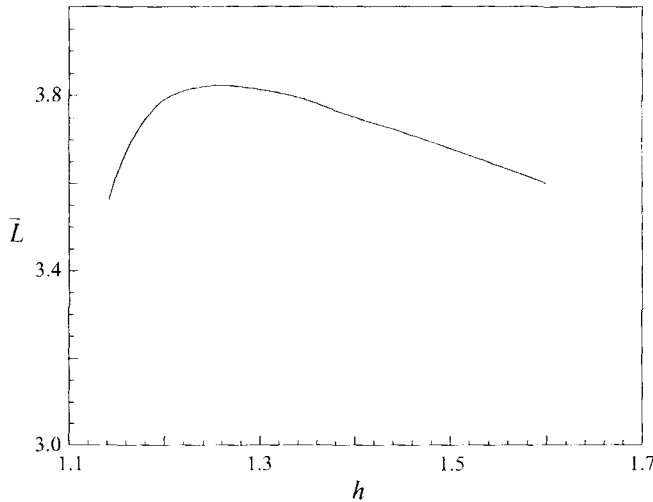


FIGURE 29. The slope $d\bar{L}/dh$ of the wavelength changes with hold-up ratio for $[\eta, R, J] = [0.8, 100, 13 \times 10^4]$. The value of β changes with h for a given \bar{L} .

predicted variation of pressure with η shown in figure 16. In this case a more positive pressure would be generated in the narrow gap which would levitate the core. The equilibrium position of the core would then be determined by a balance between buoyancy and levitation by pressure forces which, in the case of matched densities, would centre the core. In eccentric horizontal core flows of lighter-than-water oils which are in experiments, the waves in the small gap near the top wall are shorter and the positive pressures are higher than in the large gap at the bottom (see figure 30), the speed of the core is increased, the core moves to the centre and the shape of the wave tends to the axisymmetric ones studied here.

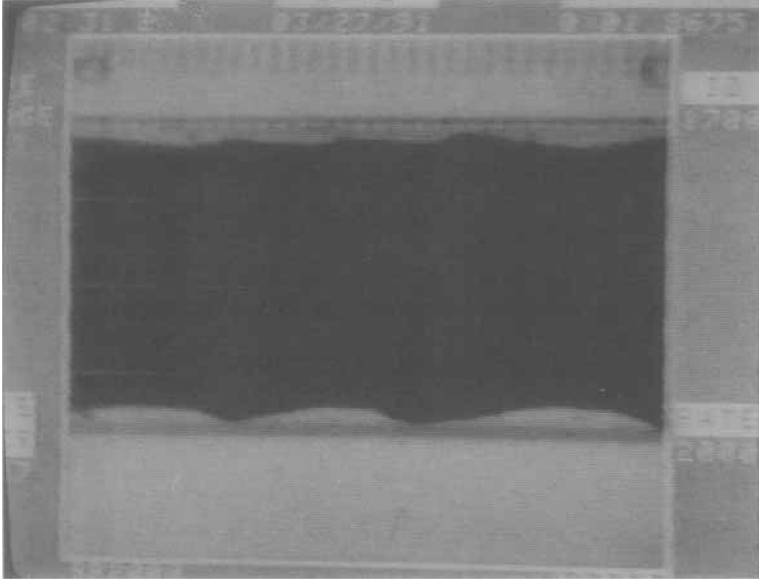


FIGURE 30. The core moves from right to left. Steep crests propagate into the water. The lighter core levitated off the top wall by high pressures produced at stagnation points at the steep slope on the top. The wave crests are closer together at the top than the bottom.

9. Lubrication theory

Lubrication theory is valid when inertia is neglected (Stokes flow), when the wave amplitude is small and the radial velocity u and $\partial w/\partial z$ are negligible. The last conditions imply that secondary motions are not present or are very weak. The required conditions can be achieved in the limit in which \mathcal{R} and $2-h$ tend to zero, in Stokes flows which perturb perfect core flows. Small gaps are one way of achieving small \mathcal{R} , but other possibilities are compatible with lubrication theory. Moreover, we have already seen (cf. figure 5 and 15) that small gaps do not give rise to long waves as is often assumed in lubrication theories. It is of value to examine the lubrication theory in bright light since it is very popular with applied mathematicians and has played a historically important role in the development of the theory of core flows.

After applying the assumptions of lubrication theory, the governing equations (3.11) reduce to

$$0 = \beta - \frac{\partial p}{\partial z} + \mu_2 \frac{1}{r} \frac{\partial}{\partial r} \left(r \frac{\partial w}{\partial r} \right). \quad (9.1)$$

where $w = 0$ at $r = f(z)$ and $w = -c$ at $r = R_2$. Hence

$$w(r) = \frac{1}{4\mu} \frac{dP_2}{dz} (r^2 - f^2(z)) - \frac{c + \frac{1}{4\mu} \frac{dP_2}{dz} (R_2^2 - f^2(z))}{\ln\left(\frac{R_2}{f}\right)} \ln\left(\frac{r}{f}\right), \quad (9.2)$$

where

$$P_2 = -\beta z + p(z) + P_2(0), \quad (9.3)$$

and

$$\frac{P_2(0) - P_2(L)}{L} = \beta. \quad (9.4)$$

The pressure difference is opposed by the integral of the shear stress on the wall,

$$\beta L \pi R_2^2 = 2\pi R_2 \int_0^L \mu_2 \frac{dw(r)}{dr} \Big|_{r=R_2} dx. \quad (9.5)$$

After combining (9.2) and (9.5), we relate the wavespeed c to the pressure gradient

$$c = -\frac{1}{4\mu_2} \frac{dP}{dz} (R_2^2 - f^2). \quad (9.6)$$

This equation can also be obtained from (4.5) with $\mu_1 \rightarrow \infty$. For a given speed c , the pressure gradient is determined by the shape of the core.

$$\frac{dP_2}{dz} = -\beta + \frac{dp}{dz} = -\frac{4\mu c}{R_2^2 - f^2(z)}. \quad (9.7)$$

Since p is a periodic function, the driving pressure gradient is given by

$$\beta = \frac{P_2(0) - P_2(L)}{L} = \frac{1}{L} \int_0^L \frac{4\mu c}{R_2^2 - f^2(z)} dz. \quad (9.8)$$

The periodic pressure, a functional of $f(z)$, is

$$p(z) - P_2(0) = \beta z - \int_0^z \frac{4\mu c}{R_2^2 - f^2(z)} dz. \quad (9.9)$$

In the perfect core-annular flow, $f(z) = R_1$ is uniform and (9.8) and (9.9) show that $p(z) - P_2(0) = 0$ and pressure gradient will be constant.

We carried out an analysis of these equation by assuming $f(z)$ and computing $p(z)$. Of course, the normal stress balance is not satisfied by the assumed shape but we could iterate all of the assumed shapes to a unique one which satisfies the reduced normal stress balance (3.13)

$$P_1 - P_2 = \frac{\sigma}{f(1+f'^2)^{1/2}} - \frac{\sigma f''}{(1+f'^2)^{3/2}}. \quad (9.10)$$

Here

$$P_1 = -\beta z + P_1(0) \quad (9.11)$$

in the core, and (9.7) implies that

$$P_2 = -\int_0^z \frac{4\mu c}{R_2^2 - f^2(z)} dz - P_2(0) \quad (9.12)$$

in the annulus. The pressure jump across the interface is then

$$P_1 - P_2 = -\beta z + \int_0^z \frac{4\mu_2 c}{R_2^2 - f^2(z)} dz + C_p, \quad (9.13)$$

where

$$C_p = P_1(0) - P_2(0).$$

Our iteration starts with any trial wave, say $f_1(z)$. Then we compute

$$P_1 - P_2 = -\beta z + \int_0^z \frac{4\mu_2 c}{R_2^2 - f_1^2(z)} dz + C_p$$

and carry out the first iteration using the normal stress balance to compute $f_2(z)$:

$$-\beta z + \int_0^z \frac{4\mu_2 c}{R_2^2 - f_1^2(z)} dz + C_p = \frac{\sigma}{f_2(1+f_2'^2)^{1/2}} - \frac{\sigma f_2''}{(1+f_2'^2)^{3/2}}.$$

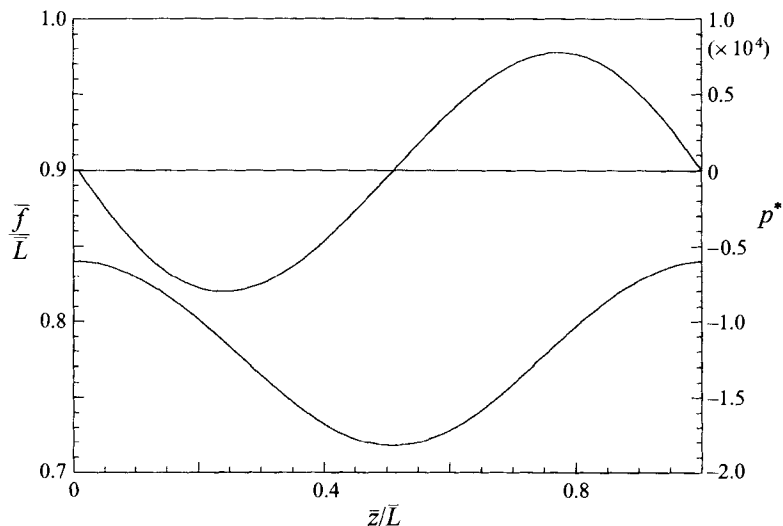


FIGURE 31. Pressure distribution and wave shape from lubrication theory when $[\eta, h, J] = [0.8, 1.9, 13 \times 10^4]$.

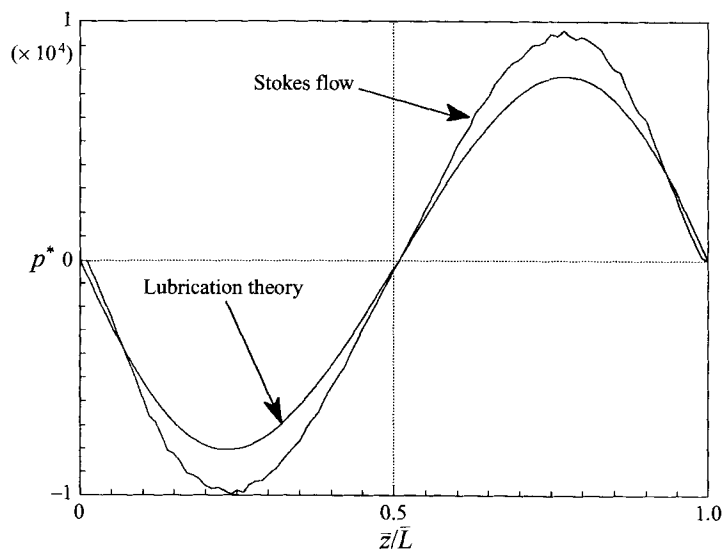


FIGURE 32. Comparison of pressure distributions when $[\eta, h, J] = [0.8, 1.9, 13 \times 10^4]$.

We then compute

$$P_1 - P_2 = -\beta z + \int_0^z \frac{4\mu_2 c}{R_2^2 - f_2^2(z)} dz + C_p$$

and so on. This iteration converges to the unique solution shown in figure 31 for each of three very different guesses for $f_1(z)$. The wave is nearly symmetric, but the pressure force is slightly negative.

Stokes flow will reduce to lubrication theory as $h \rightarrow 2$. Figure 32 compares the pressure distributions from lubrication theory and Stokes flow for the condition is specified in figure 31; in both cases the area under the pressure curve is negative. These flows, as well as those at small Reynolds numbers, may be unstable to off-centre

perturbations of the type considered by Huang & Joseph (1995) since the unbalanced core could possibly be sucked to the wall by the negative pressure force.

10. Conclusions

Core-annular flows of liquids with the same density and a high viscosity ratio were computed in a direct numerical simulation. It was assumed that flow is axisymmetric and the core is solid with advected periodic standing interfacial waves fixed on the moving core. These assumptions reduce the number of parameters defining the problem to four: Reynolds number, radius ratio, hold-up ratio and surface tension parameter. In dimensional terms, for given material parameters, we obtain solutions when the volume flow rates of oil, water and the hold-up ratio are prescribed. Only the flow rates are given in experiments and the hold-up is then determined by stability, so we are computing a family of solutions most of which are unstable.

The numerical solutions have the properties predicted by Joseph in Feng *et al.* (1995), i.e. high pressures on the forward facing slope of the wave, where the water enters into a wave. This leads to unsymmetric waves, unlike those which levitate a slipper bearing. The problem of levitation does not arise in the density matched core, but the pressure distributions which actually develop in this case seem to be such as to centre a slightly displaced core only when the Reynolds number is greater than a threshold value which depends on the parameters but in all cases is strictly positive. The concept of a threshold Reynolds number for levitation is suggested but not established by our work. To establish such a concept it would be sufficient to see if solutions for the density matched flows computed here are stable to off-centre perturbations and to compute and consider the stability of finite-amplitude off-centre core flows when the density is not matched.

This work was supported by the Department of Energy, Office of Basic Energy Science; the National Science Foundation; and the Minnesota Supercomputer Institute. The authors wish to thank Mr J. Feng, Adam Huang, Peter Huang, Terrence Liao and Walter Wang for their help and helpful discussions.

Appendix

A.1. Computational solution of the core-annular flow

The axisymmetric core-annular flow with the deformable oil core is governed by equation (3.11) subject to the normal stress condition specified in (3.13) and the force balance on the oil core described in (3.14). For each given value of the parameter triplet (c, R_1, h) , computational solution of these equations is carried out to determine the flow of water, the shape and location of the free surface of the oil core, and the wavelength. This calculation involves an iterative solution between the calculation of the flow field of water and the calculation of the free surface shape. In the following discussion, important details of these two steps and the overall solution algorithm are described.

A.2. Computation of the flow field of water

Finding the velocity and the pressure field involves the solution of the momentum and continuity equation (equation (3.11)) for the specified wave speed c and the available free-surface shape and wavelength. Relevant details of the discretization method and the solution technique and the procedure for the determination of the pressure gradient β are now described.

A.3. Discretization method and solution technique

The control-volume-based computational method of Patankar (1980) is used for the solution of the Navier–Stokes equations governing the flow of water. In this method, the domain of interest is divided into a set of control volumes. Values of scalar unknowns including pressure are stored at the main grid points. A staggered grid is used for storing the velocity components to avoid the occurrence of checker boarding of the pressure field. Thus, a normal velocity component is stored on each control volume face. This gives rise to momentum control volumes in the z - or r -directions to be displaced in the z - or r -directions, respectively. The discretization equations for z - or r -direction velocity components are constructed by integrating the z - and r -direction momentum equations over the control volumes staggered in z - and r -directions, respectively. The continuity equation is discretized over the main control volume. The convective–diffusive fluxes over the control volume faces are computed using the Power-law scheme (Patankar 1980). The resulting discretization method expresses perfect conservation over individual control volumes and the entire domain.

Two important issues need to be addressed in the application of this discretization method for predicting the flow field of water, (i) the representation of the free surface and (ii) the treatment of the periodicity conditions. In the present study, an axisymmetric cylindrical grid is used to discretize the entire domain ($0 \leq r \leq R_2$, $0 \leq x \leq L$). The rigid core is represented by imposing a zero velocity on the control volumes that lie in the oil core through the use of a high viscosity. This procedure approximates the wavy interface using a stepped grid. A grid independence study was carried out to determine the size of the grid necessary for accurate prediction of the water flow and the interface shape using an increasing number of grid points until the accuracy of the pressure distribution shows no significant change. The prediction of the core–annular flow is carried out assuming that the deformation of the wavy interface is spatially periodic. This enables us to predict the flow over the segment of the pipe corresponding to one wavelength. Thus, all variables in (3.11) are periodic at $z = 0$ and L . During discretization, the control volume faces at $z = 0$ and L are treated as topologically coincident to incorporate this periodicity condition (Patankar, Liu & Sparrow 1977).

The discretized momentum and continuity equations are solved using the SIMPLER algorithm (Patankar 1980) that addresses the velocity–pressure coupling effectively. The algorithm involves sequential solution of the pressure, momentum, and pressure-correction equations. The line-by-line method is used for the solution of the discretization equations for each variable. The circular Tri-Diagonal-Matrix-Algorithm (TDMA) is used for solution of the discretization equations along lines in the periodic direction.

A.4. Determination of the pressure gradient β

Since we have chosen to specify the wave speed c , the corresponding pressure gradient β in (3.11) has to be calculated. The condition of force balance on the oil core expressed in (3.14) provides a natural method for its determination. Thus, in each iteration of the SIMPLER procedure for calculating the water flow field, the value of β is updated according to (3.14) based on the available pressure P_2 and the shear stress τ on the free surface of the oil core. At convergence of the internal iterations for the calculation of the water flow field, the value of β is determined for the specified wave speed c and the available free-surface shape.

A.5. Determination of the free surface shape

Computational prediction of the free-surface shape involves discretization and solution of the normal stress equation with an iterative adjustment of the surface shape for obtaining the prescribed average core radius R_1 and the hold-up ratio h . Important details of these steps are now described.

A.6. Discretization and solution of the normal stress condition

The shape of the interface is governed by the normal stress and pressure jump condition reproduced below.

$$\frac{d^2 f}{dz^2} \frac{1 + \left(\frac{df}{dz}\right)^2}{f} + \frac{1}{\sigma} \left(1 + \left(\frac{df}{dz}\right)^2\right)^{3/2} (C_p - p(z)) = 0. \quad (\text{A } 1)$$

The solution of this equation is sought for the available pressure variation $p(z)$ on the free surface that is determined from calculation of the water flow field. The unknown shape $f(z)$ is represented by discrete values of f at the same locations in the z -direction used in the calculation of the flow field of water. The equations for these values of $f(z)$ are constructed by integrating the above equation over the main control volumes in the z -direction. The last term in the equation is treated explicitly as a source term and is assumed to be constant over the control volume. The resulting discretization equation has the following form.

$$a_i f_i = b_i f_{i+1} + c_i f_{i-1} + S \Delta z_i, \quad (\text{A } 2)$$

where

$$b_i = \frac{1}{z_{i+1} - z_i}, \quad c_i = \frac{1}{z_i - z_{i-1}}, \quad a_i = b_i + c_i + \frac{1 + \left(\frac{df_i^*}{dz}\right)^2}{f_i^{*2}} \Delta z_i,$$

$$S_i = \frac{1}{\sigma} \left(1 + \left(\frac{df_i^*}{dz}\right)^2\right)^{3/2} (C_p - p_i^{**}),$$

and

$$\Delta z_i = \frac{1}{2}(z_{i+1} - z_{i-1}).$$

Similarly to the flow field calculation, the periodicity of f_i values is accounted for in the above equations by recognizing that in the equation for f_N , the f_{i+1} is replaced by f_1 while in the equations for f_1 , the f_{i-1} is replaced by f_N . The single * in (A 2) represents available values that are updated within the inner iteration for determining the free-surface shape while the ** on p_i denote that these values are kept constant during the free-surface calculation and updated only in the outer iteration.

A.7. Adjustment for fixed R_1 and h

The unknown pressure jump C_p and the wavelength L provide the two degrees of freedom necessary to determine the free-surface shape consistent with the specified values of the average plug radius R_1 and the hold-up ratio h . After each iteration during calculation of the f_i values, the value of C_p is increased or decreased according to whether the available f_i values imply a value of R_1 larger or smaller than that desired. Similarly, the wavelength L is increased or decreased if the current value of the hold-up ratio h is larger or smaller than its prescribed value. The amount of adjustment in the values of C_p and L is determined using the secant method. It uses the predictions from the last two iterations to determine the sensitivity of R_1 and h to changes in C_p

and L . The sensitivity coefficients are then used for inferring the changes in C_p and L to be made in the next iteration. At convergence, this procedure provides a free surface shape and location having the desired R_1 and h for the surface pressure variation determined from the flow-field calculation.

A.8. Overall solution algorithm

The overall solution method involves an outer iteration between the flow field calculation for water and the determination of the free surface and is outlined below.

1. Prescribe the values of wave speed c , average core radius R_1 , and the hold-up ratio h .

2. Assume a free-surface shape. Calculate the velocity and pressure fields in the water region for the specified wave speed c . During each iteration of the flow-field calculation, the pressure gradient β is adjusted to satisfy the force balance on the oil plug.

3. The shape of the free surface is determined by solving the equation describing the normal stress condition for the surface pressure determined from step 2. The wavelength and the pressure jump are adjusted in each iteration so that at convergence the free surface shape is determined for the prescribed average core radius R_1 and hold-up ratio h .

4. The new free surface is now used in determining the flow field in step 2. Thus, steps 2 and 3 are repeated till convergence to obtain a self-consistent flow field of water and free-surface shape of the oil core for the prescribed values of the parameter triplet (c, R_1, h) .

The overall solution method correctly predicted the perfect core flow. Further, it predicted the same free-surface shape in the flow field of water irrespective of the initial guess surface. This constituted a rigorous test for the correctness of the computational technique. Consequently, the above method was applied for computing the details of the wavy core flow for a range of the parameter triplet (c, R_1, h) .

REFERENCES

- BAI, R., CHEN, K. & JOSEPH, D. D. 1992 Lubricated pipelining: Stability of core-annular flow. Part 5. Experiments and comparison with theory. *J. Fluid Mech.* **240**, 97-142.
- FENG, J., HUANG, P. Y. & JOSEPH, D. D. 1995 Dynamic simulation of the motion of capsules in pipelines. *J. Fluid Mech.* **286**, 201-227.
- HUANG, A. & JOSEPH, D. D. 1995 Stability of eccentric core annular flow. *J. Fluid Mech.* **282**, 233-245.
- JOSEPH, D. D. & RENARDY, Y. Y. 1993 *Fundamentals of Two-Fluid Dynamics*. Springer.
- LIU, H. 1982 A theory of capsule lift-off in pipeline. *J. Pipelines* **2**, 23-33.
- OLIEMANS, R. V. A. 1986 *The Lubricating Film Model for Core-Annular Flow*. Delft University Press.
- OLIEMANS, R. V. A. & OOMS, G. 1986 Core-annular flow of oil and water through a pipeline. *Multiphase Science and Technology* (ed. G. F. Hewitt, J. M. Delhaye & N. Zuber), vol. 2. Hemisphere.
- OOMS, G., SEGAL, A., CHEUNG, S. Y. & OLIEMANS, R. V. A. 1985 Propagation of long waves of finite amplitude at the interface of two viscous fluids. *Intl J. Multiphase Flow* **11**, 481-502.
- OOMS, G., SEGAL, A., VAN DER WEES, A. J., MEERHOFF, R. & OLIEMANS, R. V. A. 1984 A theoretical model for core-annular flow of a very viscous oil core and a water annulus through a horizontal pipe. *Intl J. Multiphase Flow* **10**, 41-60.
- PATANKAR, S. V. 1980 *Numerical Heat Transfer and Fluid Flow*. Hemisphere.
- PATANKAR, S. V., LIU, C. H. & SPARROW, E. M. 1977 Fully developed flow and heat transfer in ducts having streamwise-periodic variations of cross-section area. *J. Heat Transfer* **99**, 180.